FORMATION OF FIBERS AND SPHERES BY ELECTROSPINNING OF POLYETHYLENE OXIDE SOLUTION

By

ATUL NARASIMHAN

Bachelor of Science in Mechanical Engineering

Oklahoma State University

Stillwater, Oklahoma

2008

Submitted to the Faculty of the
Graduate College of the
Oklahoma State University
in partial fulfillment of
the requirements for
the Degree of
MASTER OF SCIENCE
May, 2009

FORMATION OF FIBERS AND SPHERES BY

ELECTROSPINNING OF POLYETHYLENE OXIDE

SOLUTION

Thesis Approved:

Dr. K.A.Sallam

Thesis Adviser

Dr. A.K. Kalkan

Dr. A.J. Ghajar

Dr. A. Gordon Emslie

Dean of the Graduate College

ACKNOWLEDGMENTS

I would like to express my gratefulness to all those who gave me the possibility to complete this thesis. My utmost gratitude goes to my thesis advisor, Dr. Khaled A. Sallam for providing me with a topic for research and then allowing me to join his team. He has been helpful and supportive at every step in my endeavor. I would specially like to thank him for his expertise, kindness, and most of all, for his patience.

I am deeply grateful to Dr. AbdelRahman El-Leathy, a visiting Assistant Professor for giving me important guidance during my first steps into research. He got me acquainted to the experimental process of electrospinning and was instrumental in obtaining the nano spheres. Another person I would like to thank is Vimal Joseph who had helped me by providing me with information on previous work done in this field.

I also wish to express my warm and sincere thanks to Anu Osta and Jaiho Lee for their timely help with the use of laser and optics during this research. I would especially like to thank Jaiho Lee for his help and contribution to the latter part of this research. I would also like to thank Dr. Kaan Kalkan and Dr. Afshin Ghajar for being part of my research committee. Finally I would like to thank my family members and friends for their constant support through the course of this journey.

TABLE OF CONTENTS

Chapter Page

LIST OF TABLES

LIST OF FIGURES

Figure Page

CHAPTER I

INTRODUCTION

1.1 Background

Studying the generation of biodegradable fibers and spheres by electrostatic atomization of biodegradable polymer solutions is of considerable interest motivated by their applications in drug delivery and tissue engineering to name a few. One method for the generation of these fibers and spheres is electrospinning. Electrospinning was discovered during the 1930's. In the electrospinning process, the polymer is dissolved into a low boiling point solvent to prepare a viscous solution. The solution is then placed into a pipette and connected to a voltage source as shown in Fig. 1.1. This induces a charge on the surface of the liquid. Mutual charge repulsion and the attraction of surface charges to the grounded collector electrode give rise to a force directly opposite to the surface tension.

As the intensity of the electric field is increased, the hemispherical surface of the fluid at the tip of the capillary tube elongates to form a conical shape known as the Taylor cone. As the intensity of the electric field is further increased, a critical value is attained at which the repulsive electrostatic force overcomes the surface tension and a charged jet of fluid is ejected from the tip of the Taylor cone. The discharged polymer solution jet undergoes an instability and elongation process. As the jet approaches the collector electrode, the solvent evaporates, leaving behind a charged polymer fiber.

The collected polymer fiber on the grounded electrode can be used to perform further analysis. Scanning electron microscope (SEM) can be used to obtain images to investigate the morphology of the obtained polymer samples. Another method that can be employed is the Transmission electron microscopy (TEM). Fig. 1.2 and 1.3 show examples of SEM and TEM images, respectively.

1.2 Problem Statement

Studying the electrospinning of a biodegradable polymer solution of Poly Ethylene Oxide (PEO) and water at different concentrations to identify the test conditions required for the formation of biodegradable spheres, beaded fibers and uniform fibers.

The main parameters that provide control over the process are as follows:

1. Electric potential (V) applied between the capillary tube containing the polymer aqueous solution and the grounded collector electrode.
2. The distance between the needle and the collector also called as gap (S) is varied using insulated threaded rods over which the collector electrode plate can be moved.
3. The concentration of the polymer solution.
4. Pressure (P) applied to the top of the capillary tube that stores the polymer aqueous solution.

1.3 Specific Objectives

1. Identifying the test conditions required for the formation of uniform fibers, beaded fibers and spheres.
2. Study the morphology of spheres and fibers using scanning electron microscope (SEM).

3. Observe the trajectory of the electrospinning jet with the help of digital holographic microscopy (DHM).
4. Observe the evolution of axis-symmetric instabilities near the injector using digital holographic microscopy.
5. Identifying the breakup regimes and the breakup regime transitions of PEO aqueous solutions under electrostatic charging.

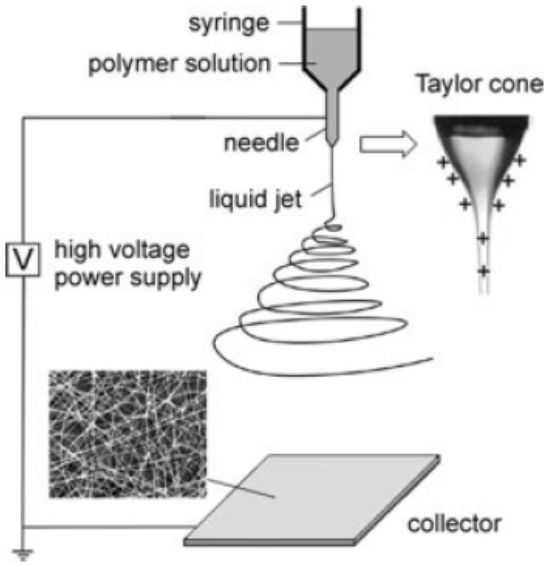

Figure 1.1 Schematic illustration of the basic setup for electrospinning (Li and Xia, 2004)

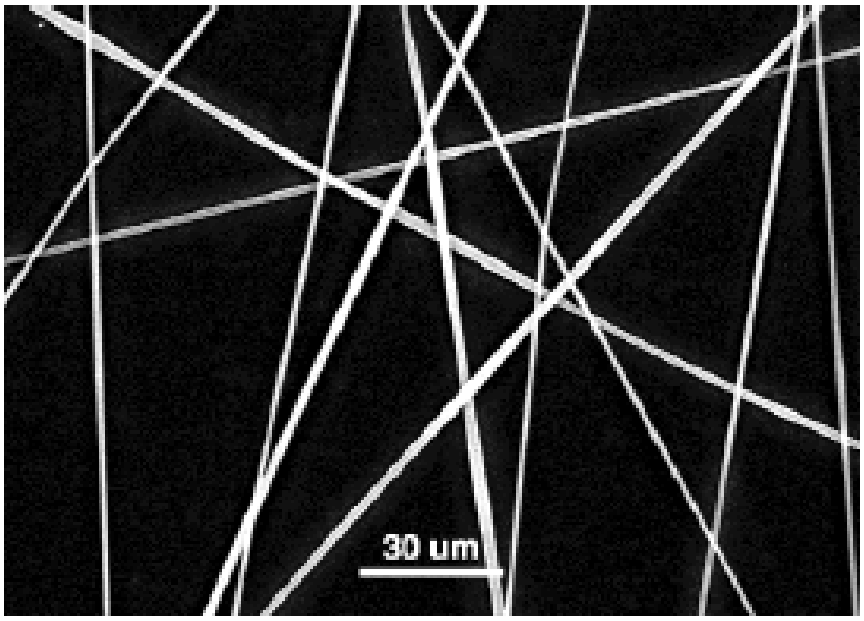

Figure 1.2 SEM image of electrospun partially crystalline poly-L-Lactide (PLLA) fiber (Bognitzki et al, 2001)

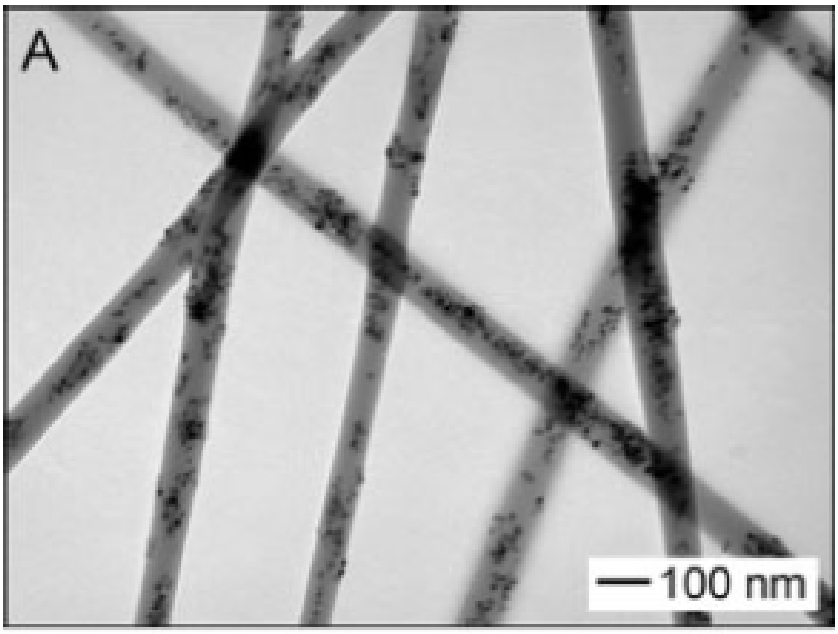

Figure 1.3 TEM image of electrospun polyvinyl pyrrolidone (PVP) nanofiber (Li and Xia, 2004)

CHAPTER II

REVIEW OF LITERATURE

2.1 Overview

This chapter describes previous studies in the fields of electrospinning. The effect of various experimental parameters on the morphology of the polymer fibers is addressed along with the applications of electrospinning.

2.2 Background

The process of electrospinning, derived from the term electrostatic spinning, was first patented by Formalas in 1934. He described the experimental setup for the production of polymer filaments using an electrostatic force. Uniform droplets of about 0.1 mm in diameter were produced from streams of highly electrified jets by Vonnegut and Neubauer in 1952. In 1971, Baumgarten made an apparatus to electrospin acrylic fibers with diameters in the range of 0.05–1.1 microns. Since 1980s the process of electrospinning has regained attention due to a surging interest in nanotechnology, as ultra fine fibers or fibrous structures of various polymers with diameters in submicron or nanometer range have been fabricated with this process. Electrospun nanofibers have been used for a number of applications such as filtration, tissue scaffolds, implant coating film and wound dressing (shown in Fig 2.1). Electrospun nanofibers with either electrical or optoelectronic properties have received much attention in recent years because of their potential uses in the fabrication of nanoscale electronic and optoelectronic devices.

2.3 Parameters affecting electrospinning

There are several parameters that affect the electrospinning process. These parameters are discussed in this section.

2.3.1 Viscosity

In 1966, Simons patented an apparatus for the production of non-woven fabrics which were ultra thin and very light in weight using electrospinning. The positive electrode was immersed into the polymer solution and the negative one was connected to a belt where the non-woven fabric was collected. He found that the fibers from low viscosity solutions tended to be shorter and finer whereas those from more viscous solutions were relatively continuous.

Electrospinning of aqueous Poly ethylene oxide (PEO) dissolved in ethanol-water solutions with viscosities in the range of 1–20 poises and surface tension between 35 and 55 dynes/cm were found to be suitable for fiber formation by Fong et al. (1999). They found that, for viscosities above 20 poises, electrospinning was prohibited because of instability in flow caused by the high cohesiveness of the solution. Formation of droplets was reported when the viscosity was low (<1 poise).

Liu and Hsieh (2002) used cellulose acetate (CA) in 2:1 acetone/ DMA (di-methyl acetamide). They found the viscosities between 1.2 and 10.2 poises suitable for electrospinning. Outside that range, the CA solutions could not be electrospun into fibers at room temperature i.e. only few fibers could be obtained from a even higher viscosity solution or the fluid jet broke up to droplets due to too low viscosity (<1.2 poise). This demonstrates that the viscosity range suitable for electrospinning of different polymer solutions is different.

During electrospinning, there may be secondary jet erupting from the main electrospinning jet [Reneker et. al. (2000)] which is stable enough to yield fibers of smaller diameter at certain viscosity. This may explain the differential fiber diameter distribution observed in some cases [Kim et. al. (2005); Demir et. al. (2002); Deitzel et. al. (2001)]. However, when the viscosity is high enough, it may discourage secondary jets from breaking off from the main jet which may contribute to the increased fiber diameter [Zhao et. al. (2004)].

Mituppatham et. al. (2004) found that the increase in concentration meant that the viscosity of the solution was strong enough to discourage the bending instability to set in for a longer distance as it emerges from the tip of the needle. As a result, the jet path was reduced and the bending instability spread over a smaller area. This reduced jet path also meant that there was less stretching of the solution resulting in a larger fiber diameter.

Although viscosity has an important role in the formation of smooth fibers, it may not determine the concentration at which fibers are formed during electrospinning. Morozov et. al. (1998) found that, for Polyethylene Oxide, the minimum concentration for smooth fiber formation was the same despite a 3.5-fold increase in viscosity.

2.3.2 Surface Tension

The initiation of electrospinning requires the charged solution to overcome its surface tension. Surface tension has the effect of decreasing the surface area per unit mass of a fluid. When there is a high concentration of free solvent molecules, there is a greater tendency for the solvent molecules to congregate and adopt a spherical shape due to surface tension. A higher viscosity will mean that there is greater interaction between the solvent and polymer molecules thus when the solution is stretched under the influence of

the charges, the solvent molecules will tend to spread over the entangled polymer molecules thus reducing the tendency for the solvent molecules to come together under the influence of surface tension.

Fong et. al. (1999), found that solvent such as ethanol with low surface tension can be added to encourage the formation of smooth fibers. Zeng et. al. (2003) proposed another way to reduce the surface tension by adding surfactant to the solution. The addition of surfactant was found to yield more uniform fibers. Even when insoluble surfactant is dispersed in a solution as fine powder, the fiber morphology is improved.

2.3.3 Solution Conductivity

The process of electrospinning involves stretching of the solution caused by repulsion of the charges at its surface. Thus if the conductivity of the solution is increased, more charges can be carried by the electrospinning jet. The conductivity of the solution can be increased by the addition of ions. When a small amount of salt or polyelectrolyte is added to the solution, the increased charges carried by the solution will increase the stretching of the solution. As a result, smooth fibers are formed which may otherwise yield beaded fibers. Zhong et. al. (2002) found that the increase in stretching of the solution will tend to yield fibers of smaller diameters. But there is a limit to the reduction in the fiber diameter. Choi et. al. (2004) reported that there will be greater viscoelastic force acting against the columbic forces of the charges, as the solution is being stretched. They also found that the increase in charge would result in greater bending instability thereby increasing deposition area of the fiber. This would also favor the formation of finer fibers since the jet path is increased.

Lin et. al. (2004) used ionic surfactants triethyl benzyl ammonium chloride to increase the conductivity of the solution at the same time reducing the surface tension. This was found to cause a reduction in fiber diameter. Another way to increase the conductivity of the solution by changing the pH of the solution was given by Son et. al. (2004). They found that under a basic condition, electrospinning cellulose acetate (CA) solution resulted in a significant reduction in fiber diameter compared to those obtained under neutral condition. Since the presence of ions increases the conductivity of the solution, the critical voltage for electrospinning to occur was also found to decrease.

2.3.4 Voltage

A crucial element in electrospinning is the application of a high voltage to the solution. The high voltage will induce the necessary charges on the solution and together with the external electric field, will initiate the electrospinning process when the electrostatic force in the solution overcomes the surface tension of the solution. Taylor (1964) found both high negative or positive voltage of more than 6kV was able to cause the solution drop at the tip of the needle to distort into the shape of a cone (Taylor Cone) during jet initiation. Depending on the feedrate of the solution, a higher voltage may be required so that the Taylor Cone is stable. The columbic repulsive force in the jet will then stretch the viscoelastic solution. If the applied voltage is higher, the greater amount of charges will cause the jet to accelerate faster and more volume of solution will be drawn from the tip of the needle. This may result in a smaller and less stable Taylor Cone as observed by Zhong et. al. (2002). When the drawing of the solution to the collection plate is faster than the supply from the source, the Taylor Cone may recede into the needle [Deitzel et. al. (2001)].

2.3.5 Feedrate

The feedrate will determine the amount of solution available for electrospinning. For a given voltage, there is a corresponding feedrate if a stable Taylor cone is to be maintained. Zhong et. al. (2002) found that the increase in feedrate resulted in a corresponding increase in the fiber diameter. This was due to the fact that there was a greater volume of solution that could be drawn away from the needle tip.

Rutledge et. al. (2001) found that there was a limit to the increase in diameter of the fiber due to higher feedrate. If the feedrate was at the same rate with which the solution is carried away by the electrospinning jet, then there must be a corresponding increase in charges when the feedrate is increased. Thus there should be a corresponding increase in the stretching of the solution which counters the increased diameter due to increased volume. Due to the greater volume of solution drawn from the needle tip, the jet would take longer time to dry. As a result, the solvents in the deposited fibers may not have enough time to evaporate given the same flight time. Therefore a lower feedrate is more desirable as the solvent will have more time for evaporation.

2.3.6 Temperature

The temperature of the solution has both the effect of increasing its evaporation rate and reducing the viscosity of the polymer solution. When polyurethane is electrospun at a higher temperature, the fibers produced have a more uniform diameter [Demir et. al. (2002)]. This may be due to the lower viscosity of the solution and greater solubility of the polymer in the solvent which allows more even stretching of the solution. With a lower viscosity, the Columbic forces are able to exert a greater stretching force on the solution thus resulting in fibers of smaller diameter [Mituppatham et. al. (2004)].

Increased polymer molecules mobility due to increased temperature also allows the Columbic force to stretch the solution further.

2.3.7 Distance between Tip and Collector

Varying the distance between the tip and the collector was found to have a direct influence on both the flight time and the electric field strength. For the formation of fibers, the electrospinning jet must be allowed sufficient time for evaporation of the solvent. Buchko et. al. (1999) reported that, as the distance between the tip and the collector was reduced, the jet had shorter distance to travel before it reached the collector plate. The electric field strength increased at the same time leading to increased acceleration of the jet towards the collector. As a result, the jet may not have enough time for the solvent to evaporate when it hits the collector.

When the distance between the tip and the collector is increased, the average fiber diameter was found to decrease [Ayutsede et. al. (2005)]. According to Reneker et. al. (2000), longer distance meant that there was a longer flight time for the solution to be stretched before it was deposited on the collector. Lee et. al. (2003) found an exception wherein with increase in distance, the fiber diameter increased. This was due to the decrease in the electrostatic field strength resulting in less stretching of the fibers. When the distance is too large, no fibers were deposited on the collector as observed by Zhao et. al. (2004).

2.4 Morphology of the fibers

During the process of electrospinning, the fibers formed often have beads. Arayanarakul et al. (2006) stated that the formation of beads along the fibers could be a result of the viscoelastic relaxation and surface tension upon the reduction of Coulombic force once

the fibers are in contact with the grounded target. Wannatong et al. (2004) stated that the occurrence of this phenomenon is likely when the charged jet is not dry enough prior to its deposition on the target, causing some parts of the charged jet to contract and form beads. When the jet is dry enough, contraction could be no longer possible, thus leaving only beaded fibers on the target. The dryness of the charged jet is controlled mainly by evaporation of the solvent during the transport of charged jet to the target. The amount of evaporating solvent is determined by a number of factors like the boiling point of the solvent, the initial concentration of the solution, the ambient condition, the size of the charged jet and the total path trajectory that the charged jet travels from the nozzle to the target.

According to Doi (1996), the polymer solutions have three concentration regimes namely the concentrated regime, the semi-dilute regime and the dilute regime. In the concentrated regime, polymer chains interpenetrate and entangle with each other, which increases the viscosity of the polymer solution. Fong et al. (1998) showed that high viscosity favors the formation of thicker fibers without beads, but surface tension drives towards the formation of beaded fibers. Electrospinning using a concentrated nylon-4,6 solution was performed by Huang et al. (2006), which produced smooth bead-free nanofibers with thicker diameters. Although the surface tension, which is one of the main factors that influenced the formation of beaded fibers, increased as the nylon concentration increased in the electrospinning solution, the viscosity increased more rapidly and was the main factor influencing the character of electrospun nanofibers.

In the dilute regime, polymer molecules have a coil-like conformation, and can be approximated by separated spheres for most descriptions of the solution behaviour. There

are many fewer polymer chain entanglements between macromolecules in a dilute solution. The viscosity of a dilute polymer solution is therefore low, approaching the viscosity of the solvent.

In the semi-dilute regime, polymer molecules act as separate coils, but are crowded and touch each other. Interactions between polymer chains therefore increase, producing significant increases in viscosity. Electrospinning in the semi-dilute regime produces nanofibers with smaller diameters, which may be beaded. The electrospinning of nylon-4,6 made from formic acid solutions of nylon at concentrations lower than 4% by weight is one such example.

Jaeger et. al. (1998) reported beaded fibers spun from aqueous solutions of poly(ethylene oxide) (PEO) and found that the bead diameter and spacing were related to the fiber diameter: the thinner the fiber, the shorter the distance between the beads and the smaller the diameter of the beads. For the formation of electrospun beaded nanofibers, solution viscosity, net charge density carried by the electrospinning jet and surface tension of the solution were referred to as the main factors. They stated that the higher viscosity favors formation of fibers without beads and higher net charge density not only favors formation of fibers without beads, but also favors the formation of thinner fibers. They also affirmed that the surface tension drives towards the formation of beads, hence reduced surface tension favors the formation of fibers without beads. Also changing the polymer concentration can vary the solution viscosity. The surface tension coefficient depends on the polymer and solvent.

Wilkes (2001) studied the effect of solution concentration, capillary–screen distance, electric potential at the tip and flowrate on electrospinning Esthane 5720, a

segmented polyether urethane. He found that bead-like structure appeared when the capillary–screen distance decreased, while the average fiber diameter was increased. When increasing the concentration, the average diameter increased and the bead-like structure turned into blobs at lower capillary–screen distance. Very high concentrations lead to failure of the fibers as the viscosity was too high. This was also attributed to high flow rates at lower concentration. Also increasing the potential decreased the fiber diameter.

Fong et al. (1998) investigated the effect of solution viscosity, charge density carried by the jet, and solution surface tension on the beaded morphology of poly(ethylene oxide) (PEO) fibers. They found that the number of beads decreased with an increase in both the solution viscosity and the net charge density and a decrease in the solution surface tension. In their experiments with PEO polymer, the polymer concentrations of 1–4.5 wt% were used. The resulting fiber membranes were visualized under SEM. For 4 wt% PEO concentration the beads were not reported to completely disappear. Instead, the bead diameters at higher concentrations were even larger and changed from spherical to spindle like shape.

Doshi & Reneker (1995) pointed out that by reducing surface tension of a polymer solution, fibers could be obtained without beads. But they also stated that this method had its limitations. Since surface tension is a function of solvent compositions and polymer concentration, different solvents would contribute to different surface tensions. However, not necessarily a lower surface tension of a solvent would always be more suitable for electrospinning.

Zong et al. (2002) obtained bead free fibers with the addition of certain filler materials into the polymer solution. They realized this while electrospinning biodegradable (D,L-lactic acid) (PDLLA) polymers. They found that with addition of 1 wt% pyridinium formate (PF) salt, the resulting nanofibers were bead-free. They argued that the addition of salts resulted in a higher charge density on the surface of the solution jet during the electrospinning, bringing more electric charges to the jet. As the charges carried by the jet increased, higher elongation forces were imposed to the jet under the electrical field, resulting in smaller bead and thinner fiber diameters. This, however, does not imply that a higher applied electrical field could result in fewer beads and smoother nanofibers. The solvent system used was also found to have a strong influence on the morphology and diameters of the as-spun cellulose acetate (CA), poly(*e*-caprolactone) (PCL), and poly(vinyl chloride) (PVC) fibers, respectively.

Zeng et al. (2003) observed significant diameter reduction and improved morphological uniformity of the as-spun poly(L-lactic acid) (PLLA) fibers were attained when a surfactant triethyl benzyl ammonium chloride, sodium dodecyl sulfate (SDS), or aliphatic PPO-PEO ether (PPO¼ poly(propylene oxide))] was added into the spinning solutions.

Huang et al. (2006) used pyridine to improve the conductivity of solutions of nylon in formic acid. Since pyridine is an organic base that reacts with formic acid to give rise to an organic salt of a weak acid and a weak base, it not only improves the conductivity of the electrospinning solution, it can also be removed easily from the resulting nanofibers by evaporation. Pyridine had a significant influence on the electrical conductivity of the formic acid solution of nylon-4,6. About 0.4% by weight pyridine

doubled the electrical conductivity of the formic acid solution of 2% nylon-4,6. This was because the pyridine in the solution increased the concentration of the current-carrying ions. The addition of pyridine also changed the interactions between the nylon molecules, thereby increasing the viscosity which helped reduce the concentration of beads. The bigger beads were no longer observed when a small percentage of pyridine was added.

Deitzel et al. (2001) found that the morphology of the fibers produced was influenced strongly by parameters such as the feed rate of the polymer solution and the applied voltage. Increasing the voltage changed the shape of the surface from which the electrospinning jet originates. This shape change, which corresponds to a decrease in the stability of the initiating jet as the voltage is increased, has been correlated with an increase in the number of bead defects forming along the electrospun fibers. They also observed that the fiber diameter increased with increasing polymer concentration according to a power law relationship. Demir et al. (2002) further found that the fiber diameter was proportional to the cube of the polymer concentration. The effect of temperature of the polymer solution was also studied by them. They found that while electrospinning polyurethane nanofibers, the fiber diameters obtained from the polymer solution at a high (70^{o}C) temperature were much more uniform than those at room temperature. But the mechanism involved has not been fully understood.

Lee et al. (2003) found that the electrospun polystyrene (PS) fibers produced an unexpected half hollowed spherical structure when tetrahydrofuran (THF) was the solvent for PS and the number of beads could be controlled by the amount of dimethylformamide (DMF) in the mixed solvents between THF and DMF.

Zou et al (2005) described the process of bead formation during electrospinning of PHBV fibers. They adopted a method to observe the morphology of the fiber near the injector. They found operating parameters like applied voltage and solution feeding rate to be important for the development of different fiber morphologies. They also found the solution properties like conductivity and surface tension to play key roles. They reported that high surface tension promoted the formation of PHBV fibers with beads, while increased conductivity favored uniform smooth fibers.

2.5 Fiber Alignment

One of the most important factors that could increase the number of applications of electrospinning is to produce continuous single nanofibers. Matthews et al. (2002) used a cylinder collector with high rotating speed as shown in Fig 2.2. They were able to align electrospun nanofibers of poly glycolic acid (PGA) (at 1000 rpm rotating speed) and type I collagen (4500 rpm rotating speed) fibers circumferentially.

Theron et al. (2001) described a novel approach to position and align individual nanofibers on a tapered and grounded wheel like bobbin as shown in Fig. 2.3. The tip-like edge substantially concentrates the electrical field so that the spun nanofibers are attracted to and can be continuously wound on the sharpened edge of the rotating wheel. With this approach, polyethylene oxide nanofibers with diameters ranging from 100 to 400 nm were aligned with the pitch varying from 1 to 2 mm. The alignment is attributed to the fact that as the nanofibers approach the electrically grounded target, they attain sufficient residual charges to repel each other. This influences the morphology of fiber depositions. As a result, once a nanofiber is attached to the wheel tip, it exerts a repulsive

force on the next fiber attracted to the tip. This mutual repulsion results in a separation between the deposited nanofibers.

2.6 Summary

From the study of the existing literature, the influence of various experimental parameters was understood. Although lots of information regarding the formation of fibers with varied morphology has been reported, there is no breakup map that describes the conditions for the formation of specific fibers. Also there is no information regarding the breakup transition when the polymer solution is subjected to electrostatic charging.

The formation of beads has been reported to be influenced by many parameters like concentration, viscosity and surface tension. But all these conclusions are based on results from scanning electron microscopy (SEM), wherein a sample is collected during the electrospinning process and is then allowed to dry before it can be considered for SEM imaging. But this drying process may actually influence the morphology of the fiber. Hence a method is to be developed that could demonstrate the variation in morphology of the fiber instantaneously.

Figure 2.1 Nanofibers for wound dressing (www.electrosols.com).

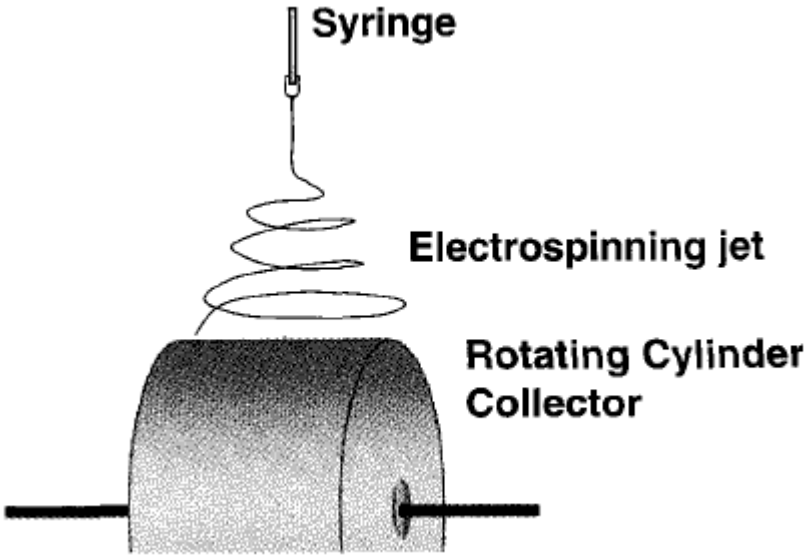

Figure 2.2 A rotating collector for electrospun ultra fine fibers (Matthews et al., 2002).

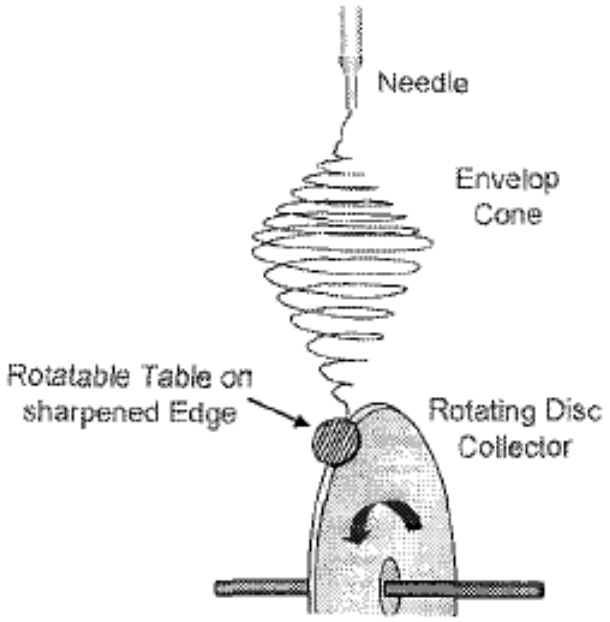

Figure 2.3 Set up used to collect uniaxial nanofibers (Theron et al., 2001)

CHAPTER III

METHODOLOGY

3.1 Overview

This chapter describes the experimental procedure and the test conditions for the implementation of electrospinning.

3.2 Apparatus

The experimentation involves two processes namely digital microscopic holography and scanning electron microscopy. The schematic illustration of the basic setup for electrospinning is shown in Fig. 1.1.

The experimental setup is shown in Fig. 3.1. There are three major components used in the process of electrospinning namely: a high voltage DC source, a cylinder with a needle of outer diameter 0.5mm, and a metallic collecting screen. The cylinder along with a nozzle is shown in Fig. 3.2. During the process, the high voltage source is used to create an electrically charged jet of polymer solution. This is performed by connecting the cylinder containing the polymers solution to the high voltage source. The collector is grounded. The cylinder containing the polymer solution is subjected to an electric field, inducing a charge on the surface of the liquid. Mutual charge repulsion causes a force directly opposite to the surface tension. As the intensity of the electric field is further increased, the hemispherical surface of the fluid at the tip of the capillary tube (needle) elongates to form a conical shape known as the Taylor cone. On further increasing the

electric field, a critical value is attained at which the repulsive electrostatic force overcomes the surface tension and the charged jet of the fluid is ejected from the tip of the Taylor cone. The discharged polymer solution jet undergoes an instability and elongation process, which allows the jet to become very long and thin. As the jet of fluid ejected from the tip of Taylor cone approaches the collector electrode, the solvent evaporates, leaving behind a charged polymer fiber. This process is performed at different conditions varying the concentration, gap and applied voltage in a systematic manner.

3.3 Instrumentation

Two different methods are used to analyze the process of electrospinning which are discussed in detail in the next two sections.

3.3.1 Digital Holographic Microscopy

The process of holography is of great importance and has wide applications in many fields. When light with sufficient coherence length (laser) is split into two partial waves by a beam splitter, one of the waves illuminates the object, which is scattered and reflected towards a recording medium e.g. a CCD (Charge coupled device) sensor while the second wave called the reference wave illuminates the sensor directly. Both these waves are made to interfere and when this interference pattern is recorded, it is called a hologram. The original object wave is then reconstructed by illuminating the hologram with the reference wave. This reconstructed image exhibits all the effects of perspective and depth of focus. This technique was invented by Gabor (1948) and later it was made practical with the use of off-axis reference beam (Leith and Upatniek (1965)), which separated the real and virtual images. With the advancements in computer technology,

Goodman and Lawrence (1967) found that holograms could be recorded on film and reconstructed digitally. Later with the development of the CCD sensor, Schnars and Juptner (1994) recorded and reconstructed holograms entirely digitally. For this experiment two different methods namely single view digital holographic microscopy and double view digital holographic microscopy were used. They are discussed in the following section.

3.3.1.a Single view digital holographic microscopy

The optical setup consisted of two frequency doubled Nd: YAG lasers (Spectra Physics Model LAB-150, 532 nm wavelength, 7 ns pulse duration). Only one laser beam was used for this experiment. The beam was passed through a polarized beam splitter cube. The resulting beam was then passed through a half wave plate and another polarized beam splitter cube, which only allows either the horizontal or vertical portion of polarized light to pass through while the other portion was reflected and directed to a beam dump located at the side of the cube. This combination of half wave plate and beam splitter cubes controls the intensity of the beam. The beam was then expanded using an objective lens (M 5x) and a 15μm pinhole and then passed directly through the test section to the CCD as shown in Fig. 3.3.

3.3.1.b Double view digital holographic microscopy

Optical setup for orthogonal double-view digital microscopic holography is shown in Fig. 3.4. A frequency doubled Nd:YAG laser was used as the light source to investigate the random motion of polymer jets in electrospinning process. Unlike the single-view digital microscopic holography setup wherein only one CCD sensor was used, two commercial grade CCD sensors (Nikon D-80 and Nikon D-70) placed orthogonally were used for

recording holograms. The laser intensity was controlled by a half wave plate. Two objective lenses (M 5x) and two spatial filters (Pinhole ~ 15μm) were used to generate expanding laser beams in the optical setup. The distance between the objective lens and the object were maintained equal for both the objective lens. Also the distance between the object and the CCD were made to be equal in both the cases.

3.3.1.c Magnification and Resolution

Digital holographic microscopy can measure very small objects by employing a spherical reference beam instead of the collimated plane beam. For good resolution of holograms, the distance between CCD and the object has to be minimized. For good holograms of high magnification, the objective lens should be put near the object and the CCD sensor should be placed far from the object. Despite this relationship between magnification and resolution of holograms, the total distance from the objective lens to the CCD sensor plays the most primary role in reconstructing holograms. A commercial grade CCD (Nikon D-70) was used for holographic recording.

After the hologram was recorded, it was reconstructed using the convolution type approach which solves the Rayleigh Sommerfeld formula for reconstruction of a wave field. Digital magnification can be introduced during the reconstruction after the hologram has been recorded. This was done by manipulating the equations used in reconstruction. The manipulation comes in the form of relocating the virtual source point used in reconstruction. However, this does not improve the actual resolution of the image. The actual resolution is controlled by the distance from the object to the CCD, the wavelength of the light, and the pixel size of the CCD.

The relation between resolution, magnification and best working distance were established using a 1951 resolution target as shown in the Fig. 3.5. The reconstructed image is shown in Fig. 3.6. The resolution (R) and best reconstruction distance (D) at different magnifications (M) were obtained. The results for the four magnifications namely M=1, 2, 4 and 8 were plotted on a graph, which is shown in Fig. 3.7. The graph depicts that the resolution decreases as magnification increases. Also the best reconstruction distance increases with the increase in magnification. From these results it was inferred that lower magnification was most suitable for the experimental procedure.

3.3.1.d Spatial Calibration

After the digital hologram is stored on the CCD sensor, it was reconstructed by a numerical algorithm. After the reconstruction process, the three-dimensional hologram is expressed as many reconstructed two-dimensional image planes. A spatial calibration was made to determine what actual length each pixel represents. In ordinary 2-D techniques, image of an object of known dimensions would be captured and a global calibration could be applied. However, this same technique can not be used for the DMH because objects closer to the CCD sensor appear larger than those farther away because of the use of expanding laser beam in the recording process. To solve the problem five pins were used to determine the spatial calibration at different reconstruction distances. Each pin had a diameter of 0.5mm; the spacing among them was 5mm as shown in Fig. 3.8. The hologram of the calibration pins was obtained and reconstructed. The image of different pins was focused best in different 2-D planes. When one pin was focused at a particular 2-D plane, the others were out of focus. Although the pins have the same physical diameter, the pixel numbers of the reconstructed pins are different from each

other. The reconstructed image of the nearest pin to the CCD sensor was the smallest. The relationship between the ratio of the measured pin diameter (dm) to its reconstructed pin diameter in pixels (dr) versus the reconstruction distance was obtained. The linear function for the spatial calibration could be determined from the best fit curve of the data obtained. The actual dimensions of the electrospinning jet can be determined with this linear equation. This equation will vary for different optical setup and a new calibration has to be performed each time. A more detailed description of digital holographic microscopy and spatial calibration process has been done by Lee et. al. (2008).

3.3.2 Scanning Electron Microscopy

This method was utilized to observe the morphology of the charged polymer obtained on the collector electrode. A small circular piece of copper was placed in the centre of the collecting electrode. During the electrospinning process, some part of the polymer jet would deposit on the piece. This piece was later used as sample for obtaining SEM images. Samples were obtained for each test condition. To obtain SEM images from the sample, the samples were first irradiated with a finely focused electron beam. A signal was obtained in the form of back scattered electrons and this signal was used to examine various characteristics of the sample. For obtaining the SEM images for this experiment, the scanning electron microscope at Oklahoma research park, Stillwater was used. Because the polymer fiber was non-conductive, it had to be coated with an ultrathin layer of electrically-conducting material. The material used for coating was gold and was deposited by high vacuum evaporation of the sample. Once the samples were ready for scanning electron microscopy, many SEM images with varying magnifications were

obtained. These images were then analyzed using Sigma scan. Sigma Scan was used to measure the diameter of the beads and spheres along with their tail lengths.

3.4 Test Conditions

PEO, with an average molecular weight of 9 $x10^5$ g/mol and distilled water (solvent) were used to prepare the polymer solution. The solutions were prepared at room temperature, and gently stirred to accelerate dissolution and to obtain solutions of different concentrations. A list of all the conditions at which electrospinning was performed is shown in the table 3.1.

Test Con-ditions	PEO (g)	Water (g)	Applied Voltage (kV)	Gap S (m)	Viscosity (centipoise)	Surface tension (mN/m)	RH %	T (^{0}C)
1	4	100	20	0.19	1250*	76.6*	25	24
2	2	100	20	0.19	126	58.23	25	24
3	1	100	20,30	0.17, 0.23	13*	77.8*	25	24
4	0.5	100	20,30	0.17, 0.23	6.46	61.58	25	24
5	0.25	100	20,30	0.17, 0.23			25	24

Table 3.1 Test conditions at which the experiments were performed.

***** Data obtained from Fong et al. (1998)

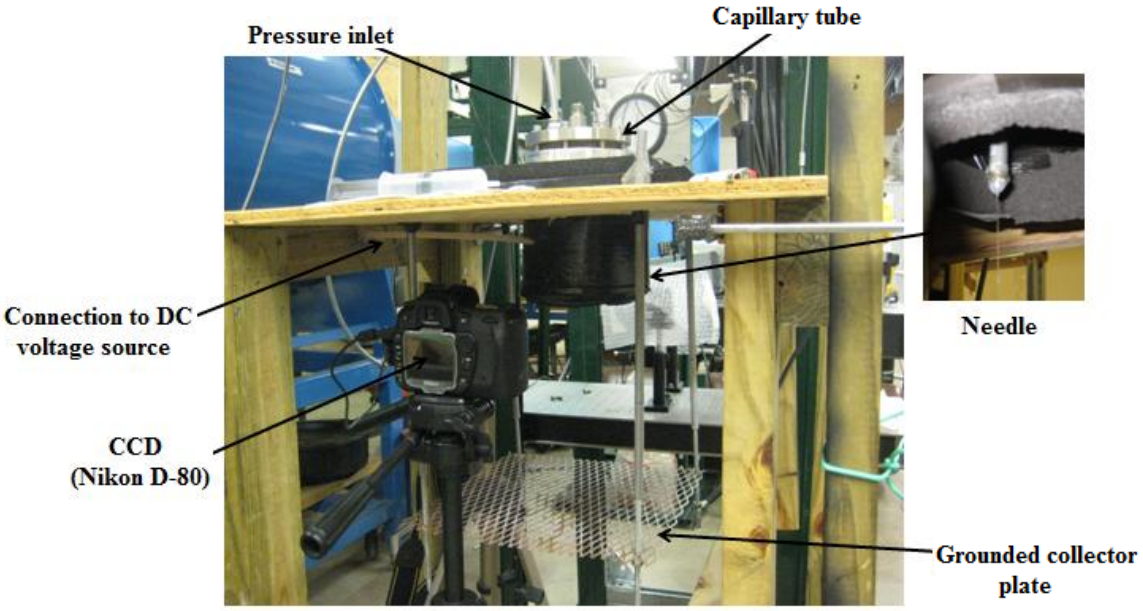

Figure 3.1 Experimental setup for electrospinning

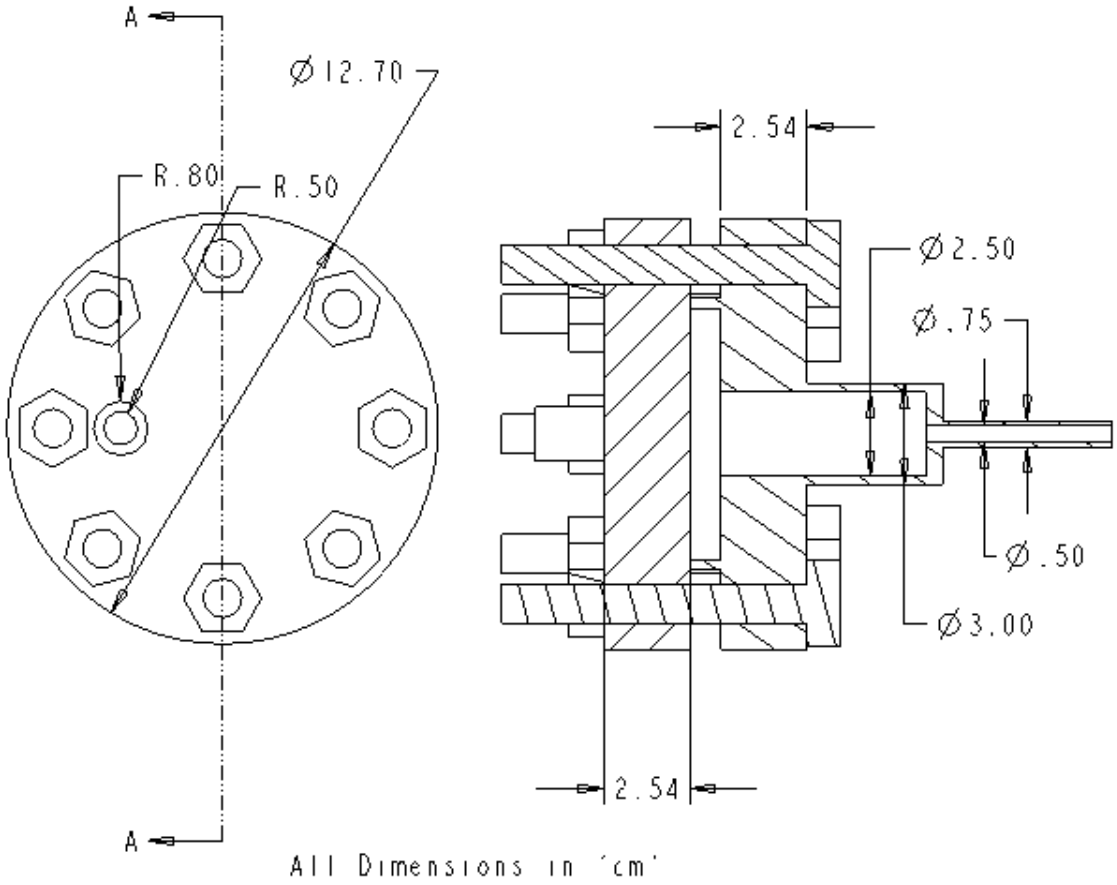

Figure 3.2 Cylinder for storing polymer solution

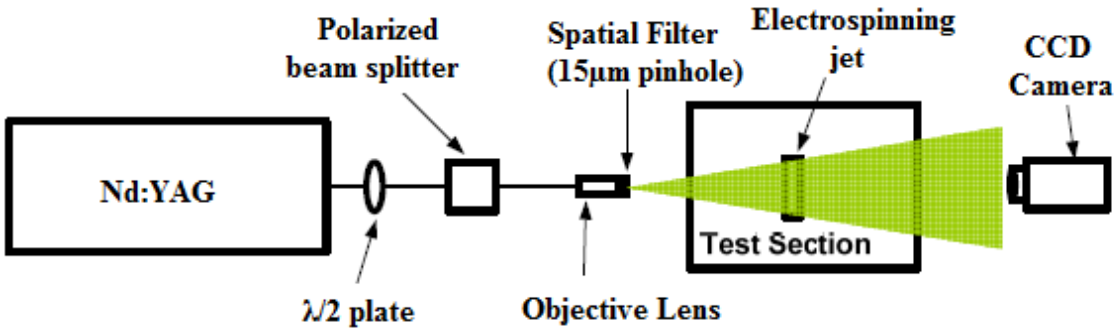

Figure 3.3 Schematic illustration of single view digital holographic microscopy.

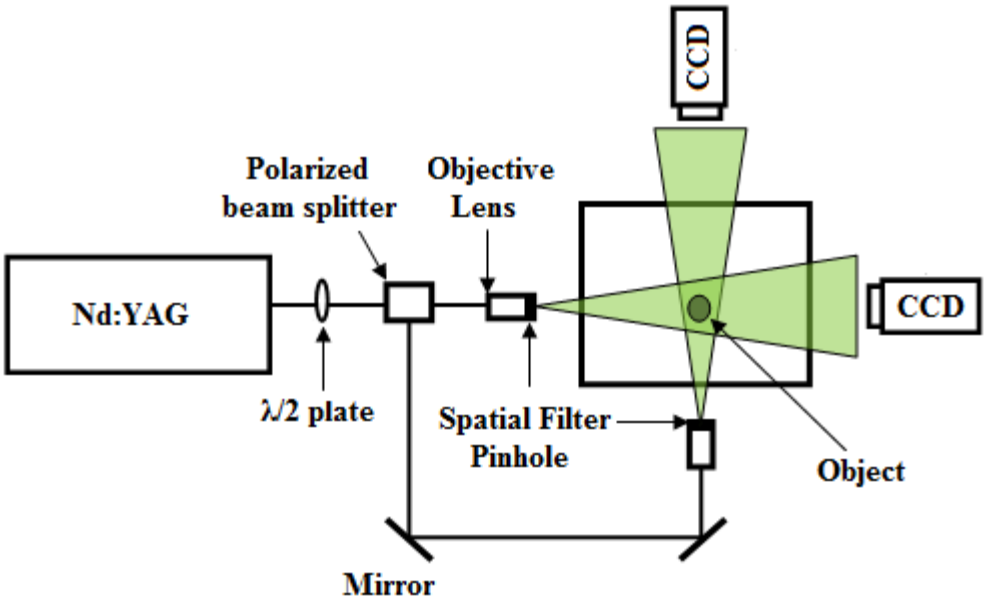

Figure 3.4 Schematic illustration of double view digital holographic microscopy.

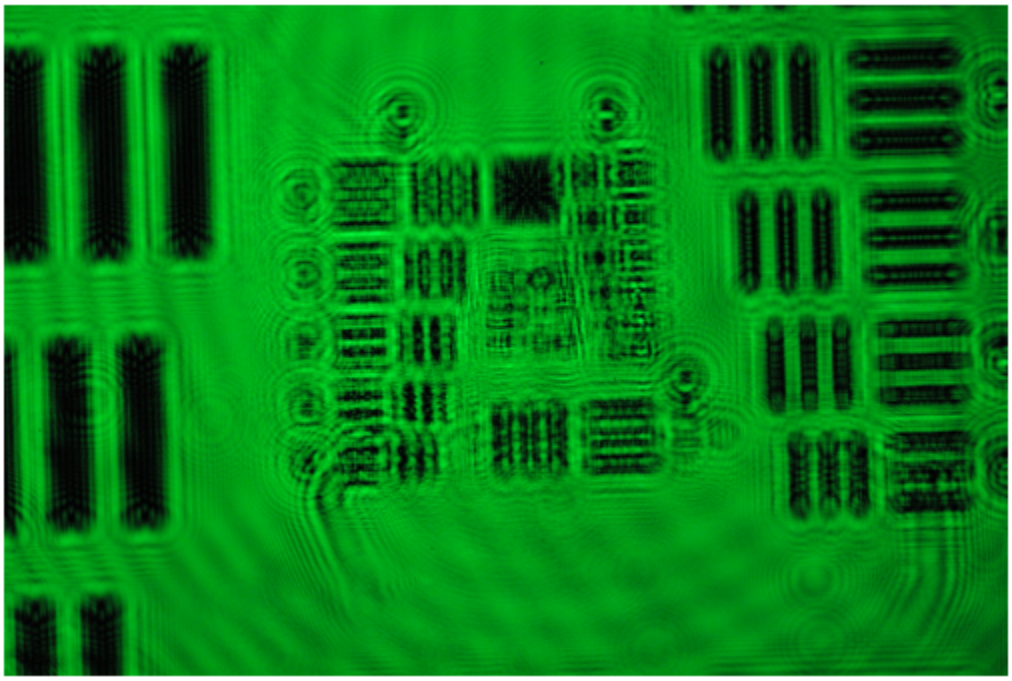

Figure 3.5 Hologram of a 1951 resolution target.

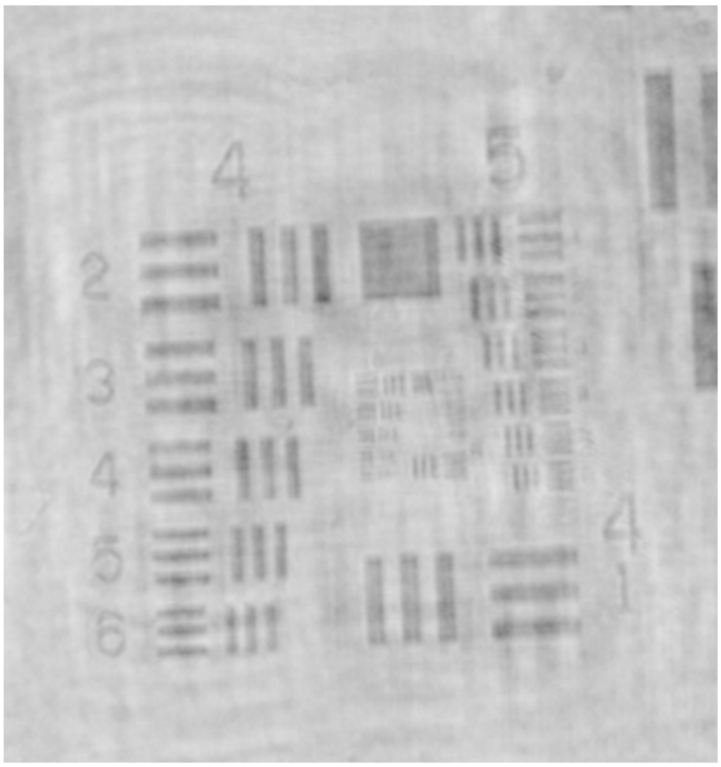

Figure 3.6 Reconstructed hologram of 1951 resolution target.

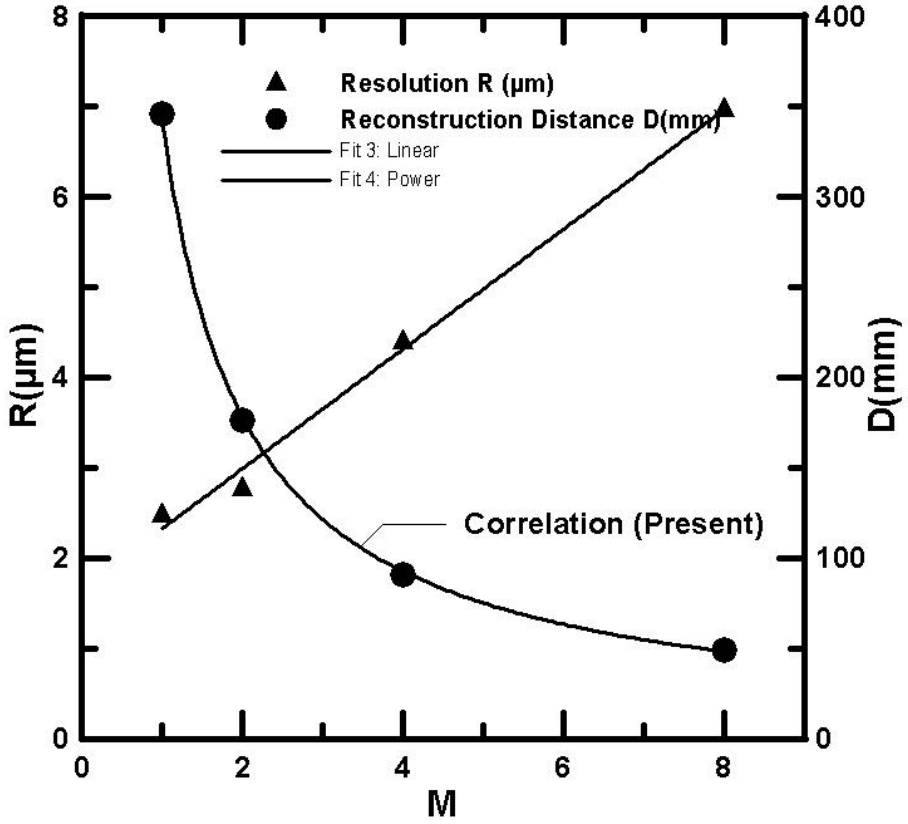

Figure 3.7 Effect of magnification on resolution and reconstruction distance.

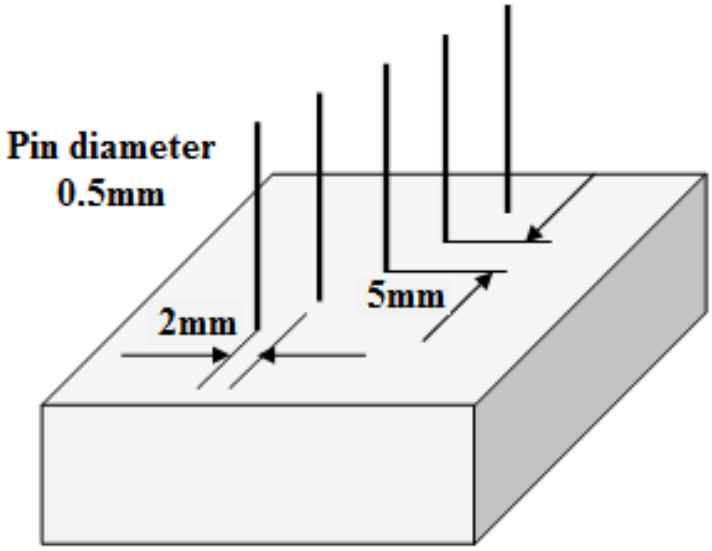

Figure 3.8 Schematic of pins used for the scale calibration of reconstructed holograms
.

CHAPTER IV

FINDINGS

4.1 Overview

In this chapter the results from the digital holographic microscopy for both single view and double view holographic microscopy are shown. Scanning electron microscopy results are discussed in detail. The effects of various experimental parameters on the morphology of the electrospun polymer are observed using SEM images. Also the condition at which the formation of spheres was first seen and the conditions at which beaded and non-beaded polymers were observed is reported.

4.2 Flow Visualization

Polymer solutions of three different concentrations were considered for this study. After the capillary tube was filled with a polymer solution of 0.5%w/v, the image in Fig. 4.1 was obtained upon reconstruction of the hologram. Since the voltage had not been applied, the polymer solution formed a spherical droplet at the tip of the needle whose outer diameter was 0.5mm. Once the DC voltage source was applied for a voltage of 5kV, while keeping the gap(S) = 0.23m, the image in Fig. 4.2 was obtained. From the image it can be seen that the spherical droplet from Fig. 4.1 is trying to change its form into a cone. When the same conditions were allowed to prevail for some time, the image in Fig. 4.3 was obtained. From the image the formation of the Taylor cone was apparent. During this entire process, there was no external pressure applied on the capillary tube.

Due to absence of external pressure, a constant Taylor cone was not possible. As soon as the voltage was increased to 10kV, keeping the gap constant, the image in Fig. 4.4 was obtained. Two noticeable aspects of the image in Fig. 4.4 are the absence of Taylor cone and the deviation of the jet from the center of the nozzle. The trajectory of the electrospinning jet was simulated by Yarin et. al.(2001). The trajectory obtained from the simulation is shown in Fig. 4.5(a). To see the electrospinning of the jet over a larger area, the field of view was changed by moving the CCD sensor closer to the needle tip. The image in Fig. 4.5(b) shows the electrospinning of a 0.5%w/v PEO polymer for V= 5kV and S = 0.23m. This experimental result substantiates the simulation performed by Yarin et. al. (2001).

The polymer concentration was increased to 2%w/v and the effect of pressure on the polymer solution was observed. When a voltage of 5kV for S = 0.23m was applied to the polymer solution, the image in Fig. 4.6 was obtained. From the image, the bending instability of the jet is visible. When a pressure of 1psi was applied to the capillary tube and the voltage and gap were maintained constant, the image in Fig. 4.7 was obtained. From the image it can be seen that the diameter of the jet at nozzle exit is larger. Also the bending instabilities are not seen for the same field of view. When a polymer solution of 4%w/v was considered, for V=20kV, S = 0.23m and pressure at 3psi, the image in Fig. 4.8 was obtained. From the image it can be seen that the Taylor cone is still prevailing even though the voltage is as high as 20kV. The concentration of the polymer and the pressure could be the reasons for this to occur.

In double view digital microscopic holography, a 2%w/v polymer was considered. A small pressure of 0.25psi was applied to the capillary tube and a voltage of 5kV was

applied to the polymer solution while the gap was 0.23m. Since two CCD sensors placed orthogonally were used, two images were obtained for the same time instance. The image in Fig. 4.9 shows the front and side view of the electrospinning jet. There is a small difference in the size of the two images because the sensor size of Nikon D80 is larger than that of Nikon D70.

The SEM images of non beaded and beaded fibers are shown in Fig. 4.10 and 4.11 respectively. The images show that the beads are formed when the concentration of the PEO solution is 2%w/v. The result clearly illustrates that the initial concentration of the polymer solution affect the morphology of the deposited polymer fibers. The reason for the polymer to form a bead free fiber at the test conditions of Fig. 4.10 may be attributed to the increased damping of the jet instabilities. The bead-free fibers were generated using a polymer solution with a concentration of 4%w/v in the Fig. 4.10. The beaded fibers were generated using a polymer solution with a concentration of 2%w/v as shown in Fig. 4.11.

4.3 Effect of Experimental Parameters

For a given concentration of the polymer solution, the voltage and gap were varied to obtained different sets of test conditions as shown in table 3.1. A graph representing the relationship between surface tension and concentration was plotted. On the same graph the polymer viscosity for varying concentrations was plotted. This graph is shown in Fig. 4.12.

For a polymer concentration of 1%w/v i.e. 1gm of PEO in 100ml of water, the SEM images are shown in Fig. 4.13. The image on the top represents the conditions at which the gap is 0.17m and the applied voltage is 20kV. The lower image represents the

test condition at which the gap is 0.23m and the applied voltage is 30kV. From the images it is apparent that the long fibers were observed at lower voltage and smaller gap whereas the formation of sphere-like structures and small “satellite” spheres were observed for higher voltage and larger gap.

For a polymer concentration of 0.5%w/v, four different test conditions were used to obtain the SEM images as shown in Fig. 4.14. Two gaps of 0.17m and 0.23m and two applied voltage of 20kV and 30kV were used to generate the four test conditions as shown. Spheres with long tails were observed at lower voltage and smaller gap. As the voltage was increased, shorter tail lengths along with satellite spheres were observed. For a larger gap of 0.23m and a higher voltage of 30 kV, the tail length decreased and droplets of submicron range were first observed.

As the concentration of the polymer solution was reduced to 0.25%w/v, there was further reduction in the tail length. This is depicted by the SEM image shown in Fig. 4.15. The image in the top row represents the test condition at which gap is 0.17m and the applied voltage is 20kV. As the distance between the electrodes was increased to 0.23m, the sphere formation was more apparent with further reduction in the tail length. This is shown by the left SEM image in the second row. When the voltage was further increased to 30kV, the formation of spheres without any tail was observed.

The diameters and the tail length of the droplets were measured from the SEM images using Sigma Scan. Three parameters namely the average diameter (d_{avg}), ratio of tail length (L) to d_{avg} and e (the ratio of maximum diameter to minimum diameter) were obtained. These parameters along with their uncertainties were plotted against the ratio of

applied voltage (V) and gap (S) and are shown in Fig. 4.16. The data used to plot this graph is included in appendix.

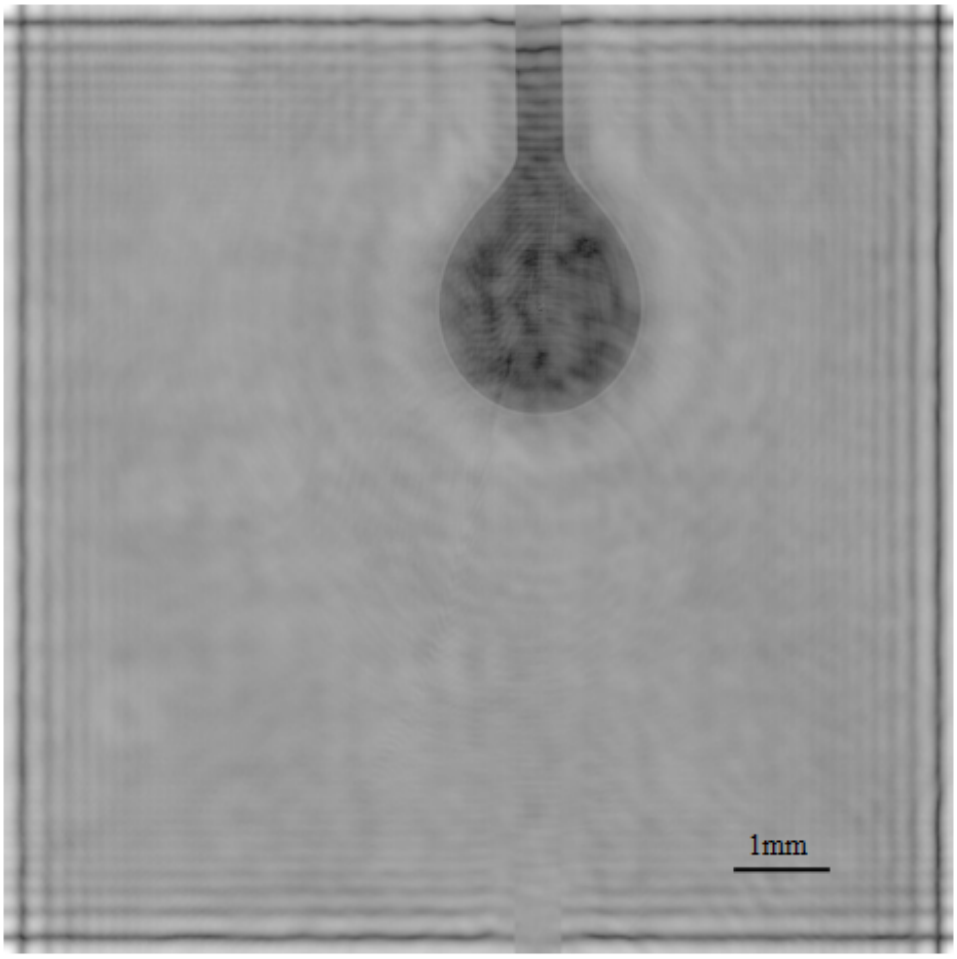

Figure 4.1 Concentration=0.5%w/v, Voltage V=0kV, S=0.23m, Pressure=0psi.

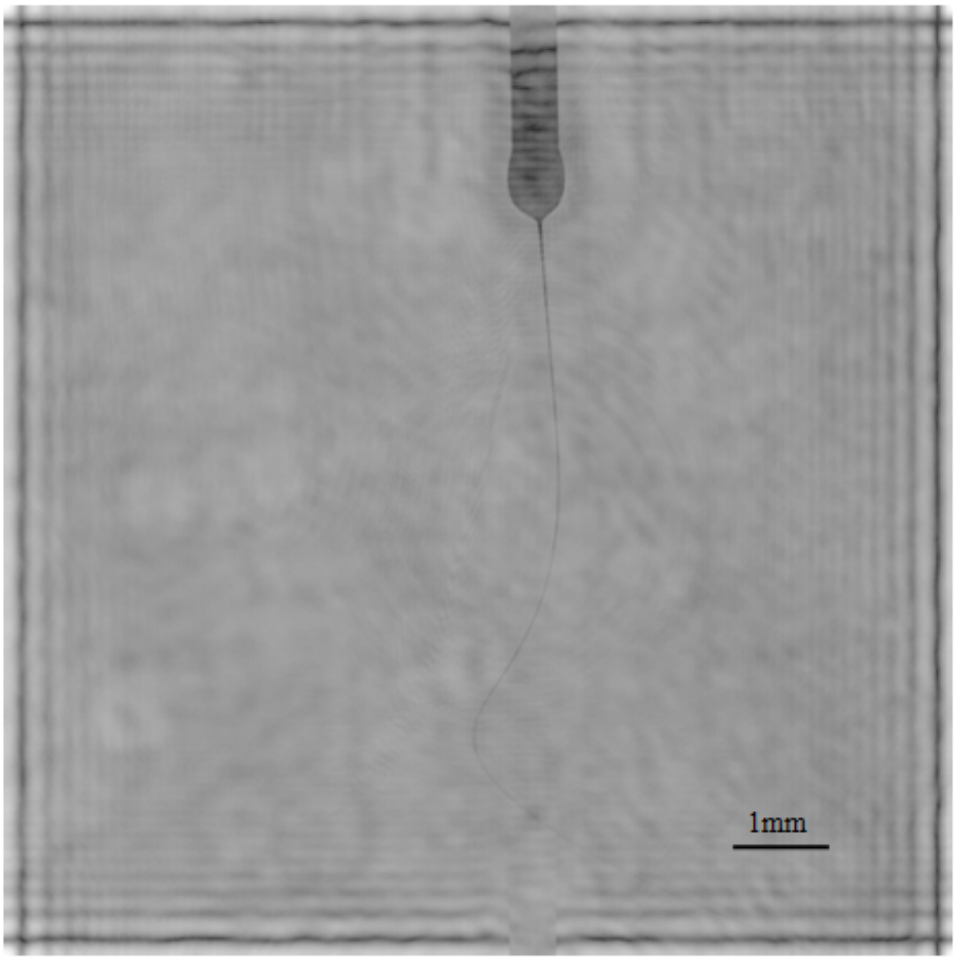

Figure 4.2 Concentration=0.5%w/v, Voltage V=5kV, S=0.23m, Pressure=0psi.

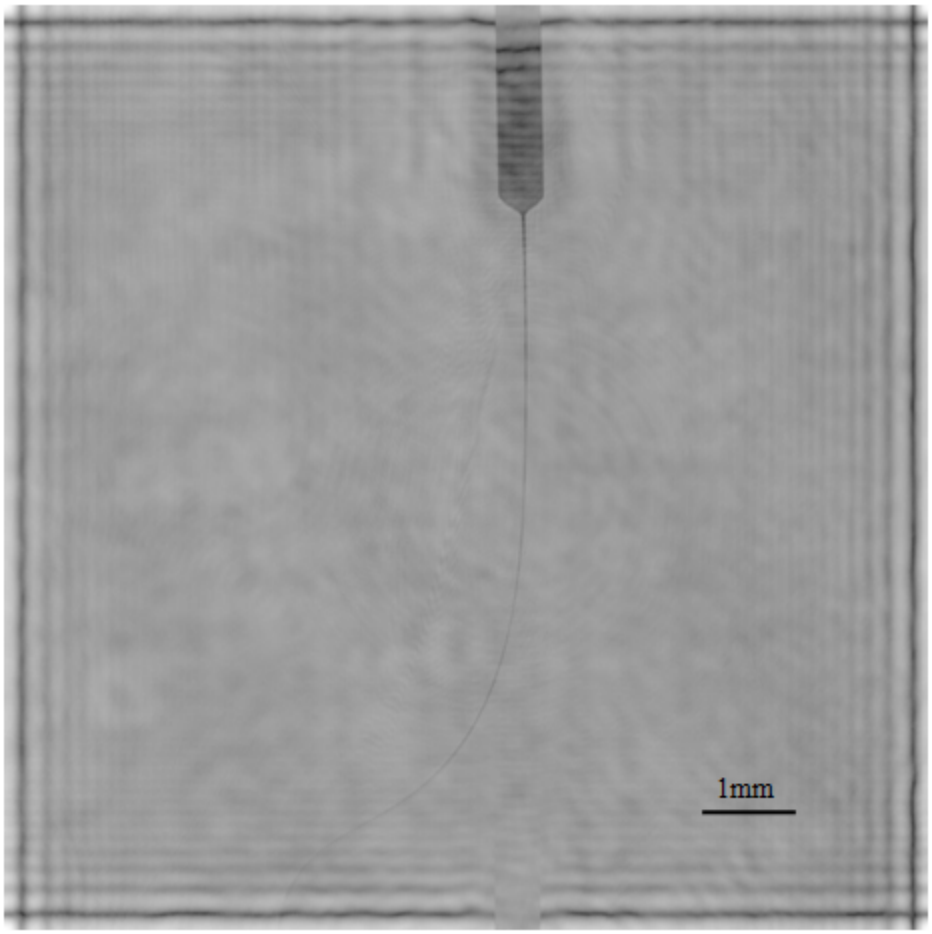

Figure 4.3 Concentration=0.5%w/v, Voltage V=5kV, S=0.23m, Pressure=0psi.

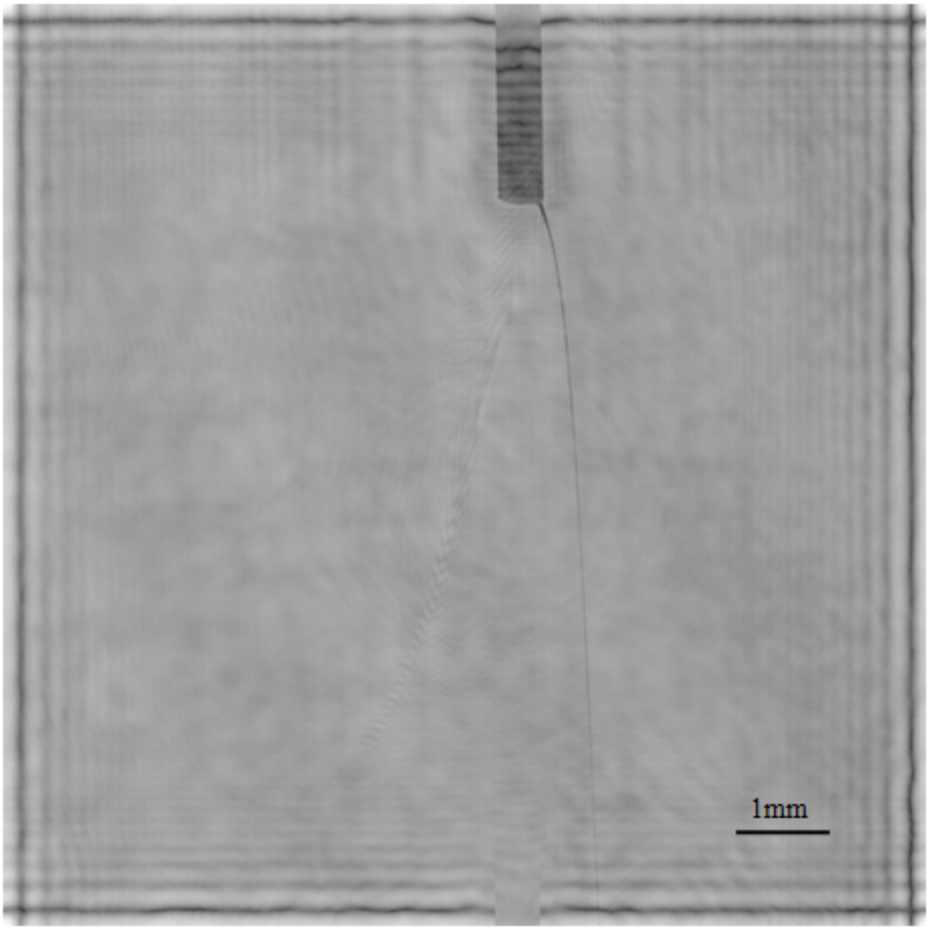

Figure 4.4 Concentration=0.5%w/v, Voltage V=10kV, S=0.23m, Pressure=0psi.

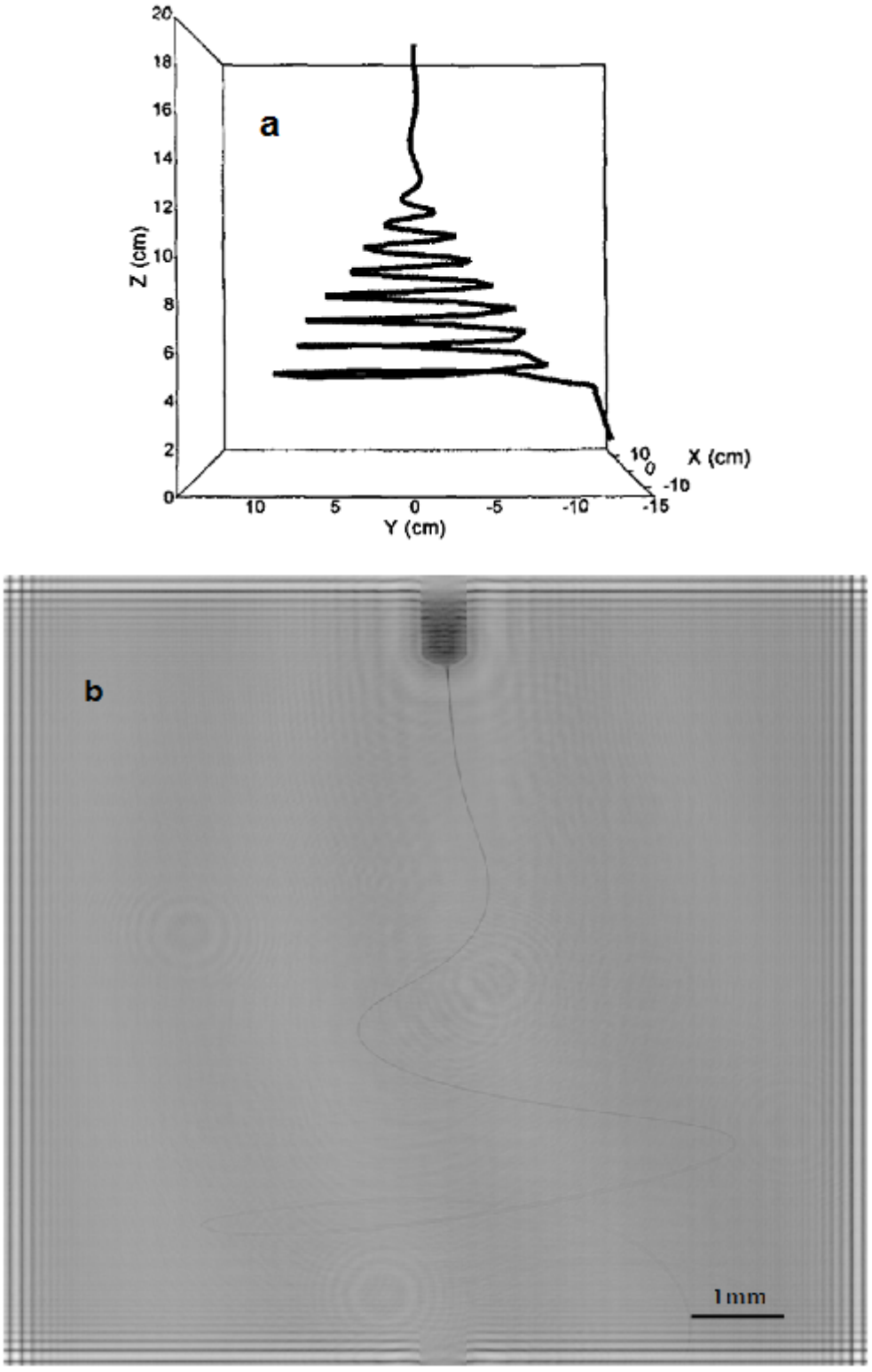

Figure 4.5 (a) Simulation of trajectory performed by Yarin et. al. (2001), (b) Larger field of view. Concentration=0.5%w/v, Voltage V=5kV, S=0.23m, Pressure=0psi.

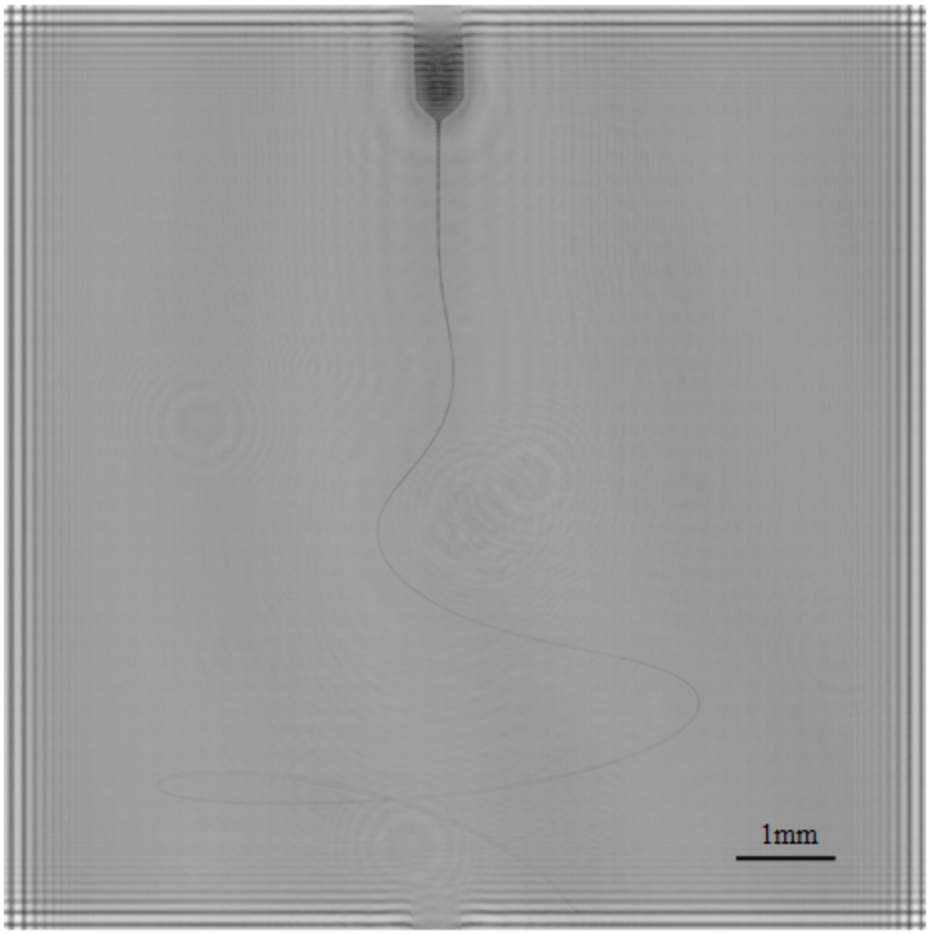

Figure 4.6 Concentration=2%w/v, Voltage V=5kV, S=0.23m, Pressure=0psi.

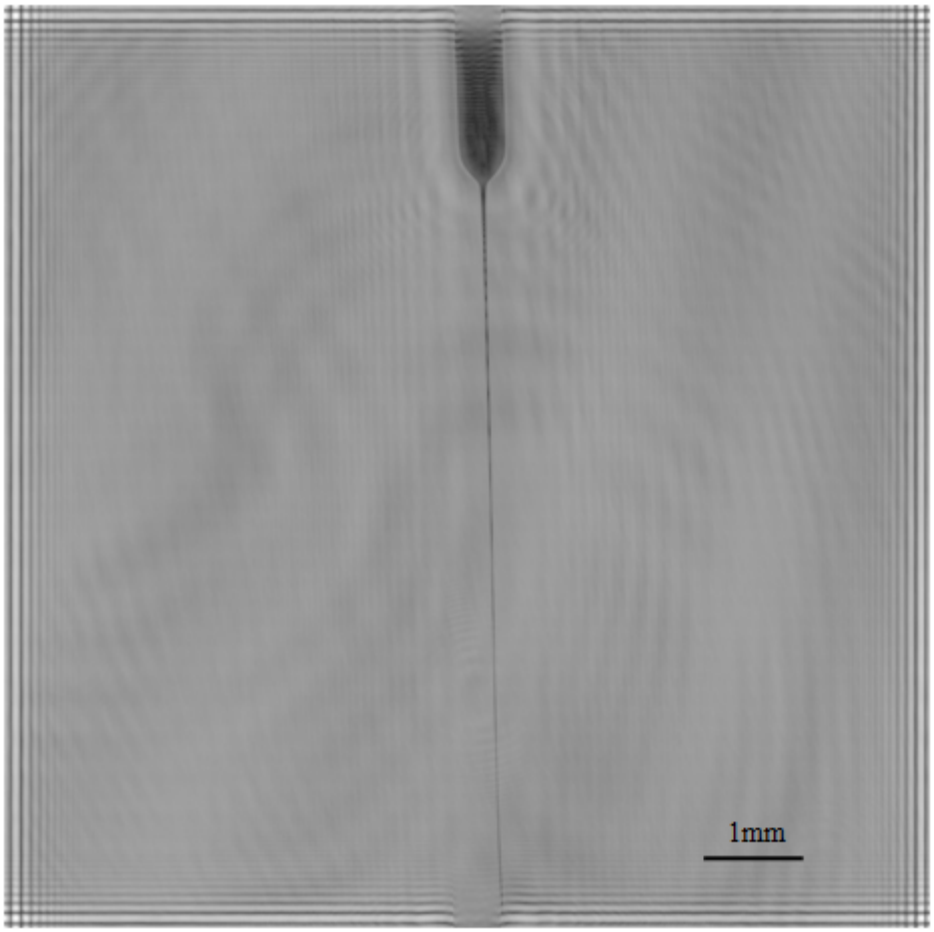

Figure 4.7 Concentration=2%w/v, Voltage V=5kV, S=0.23m, Pressure=1psi.

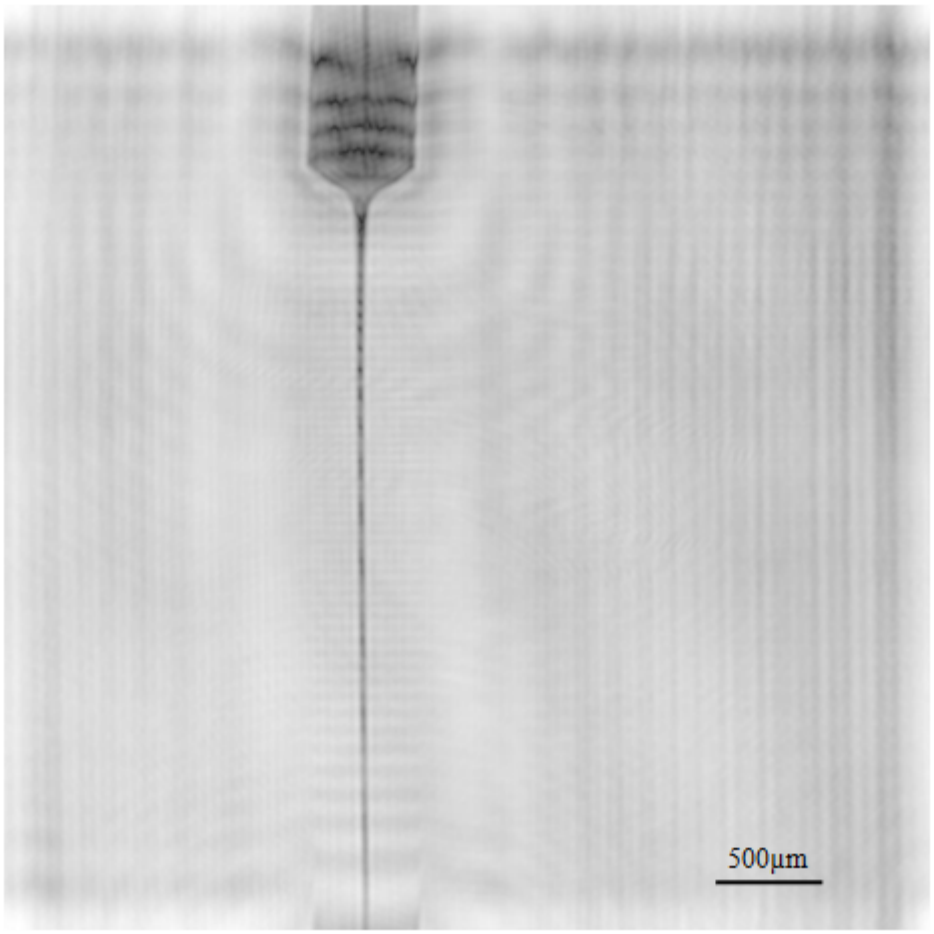

Figure 4.8 Concentration=4%w/v, Voltage V=20kV, S=0.23m, Pressure=3psi.

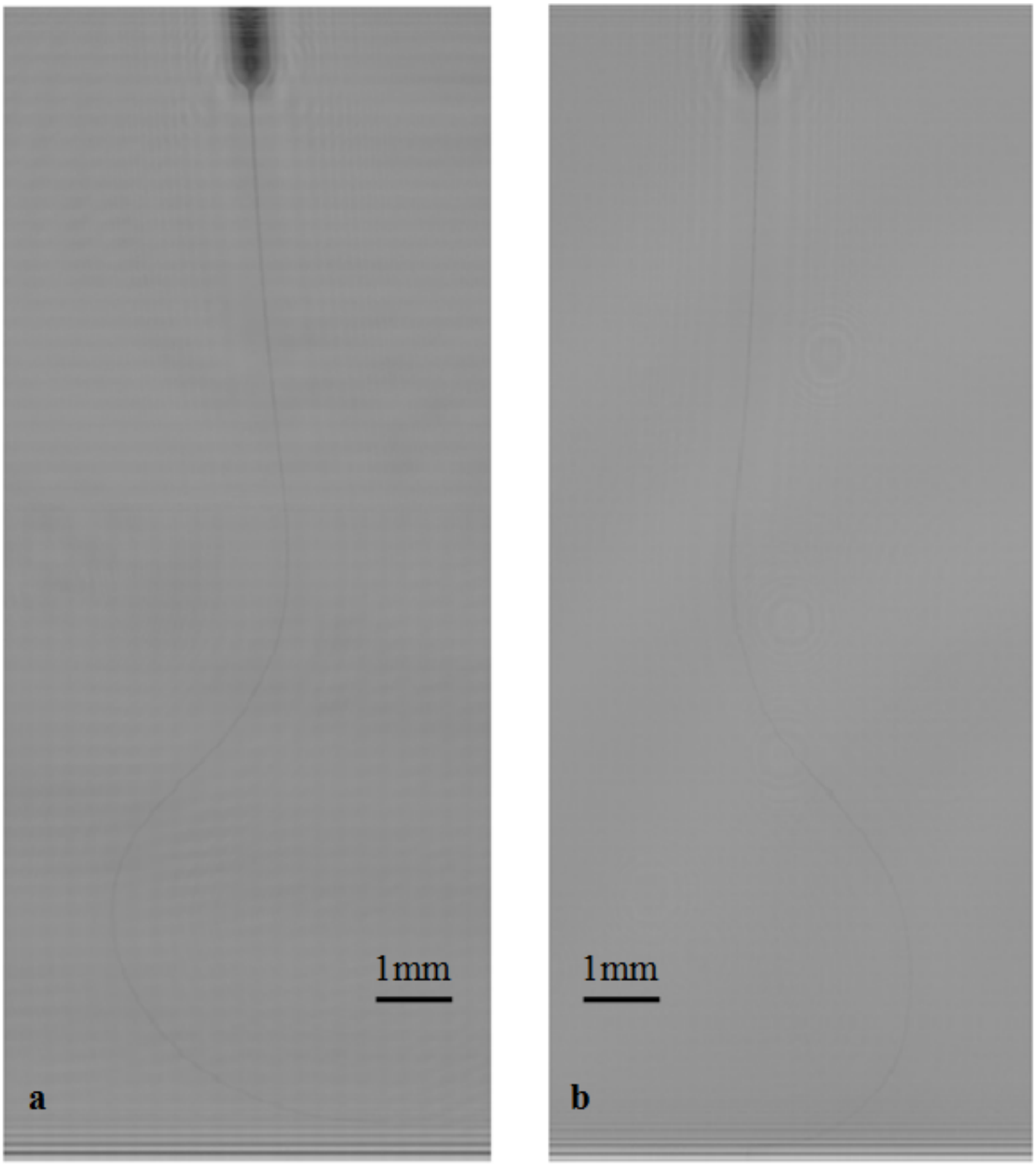

Figure 4.9 Double view digital holographic microscopy. (a) Front view. (b) Side view. Concentration=2%w/v, Voltage V=0kV, S=0.23m, Pressure=0psi.

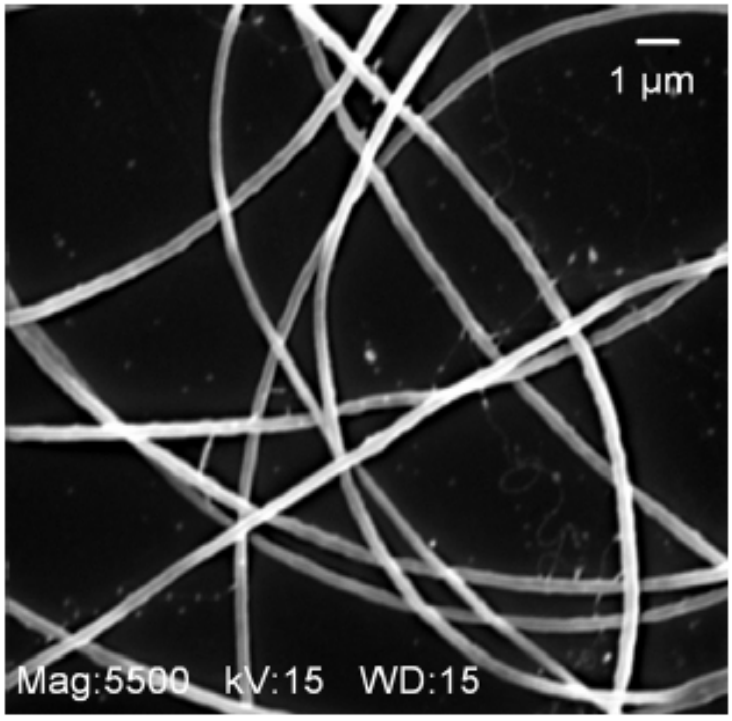

Figure 4.10 SEM image showing non beaded fibers for polymer concentration of 4%w/v.

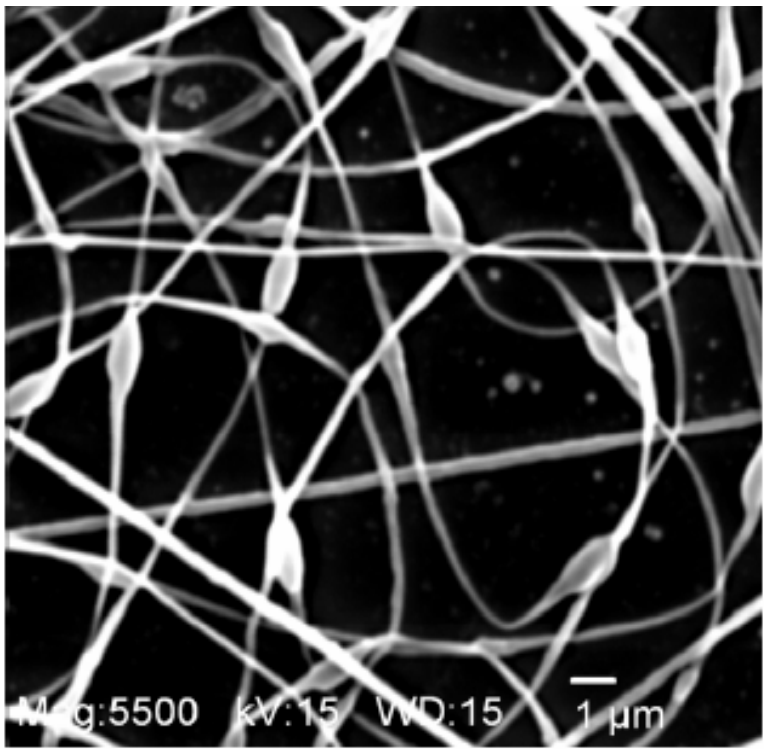

Figure 4.11 SEM image showing beaded fibers for polymer concentration of 2%w/v.

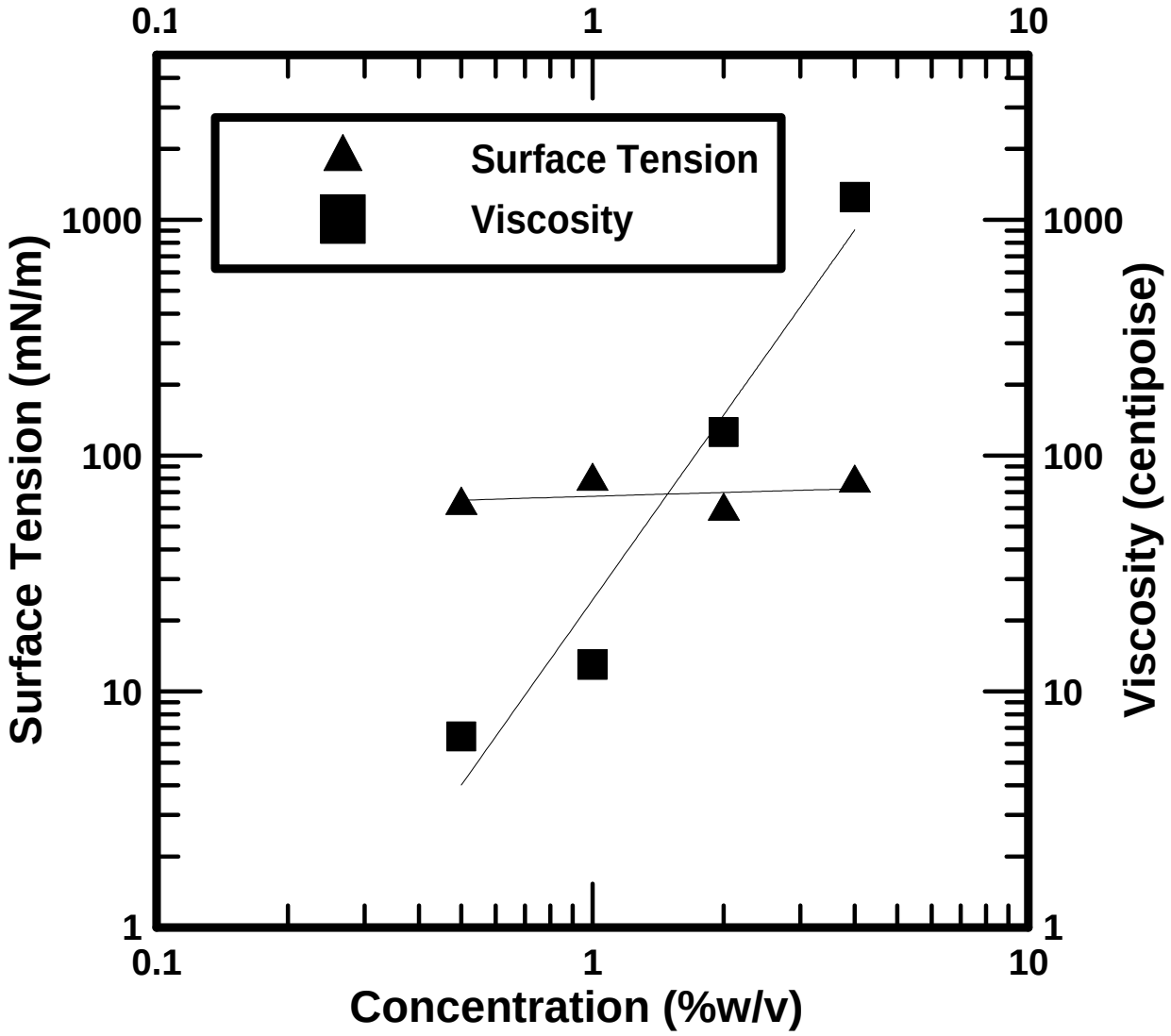

Figure 4.12 Graph representing Concentration Vs Viscosity and Concentration Vs Surface tension

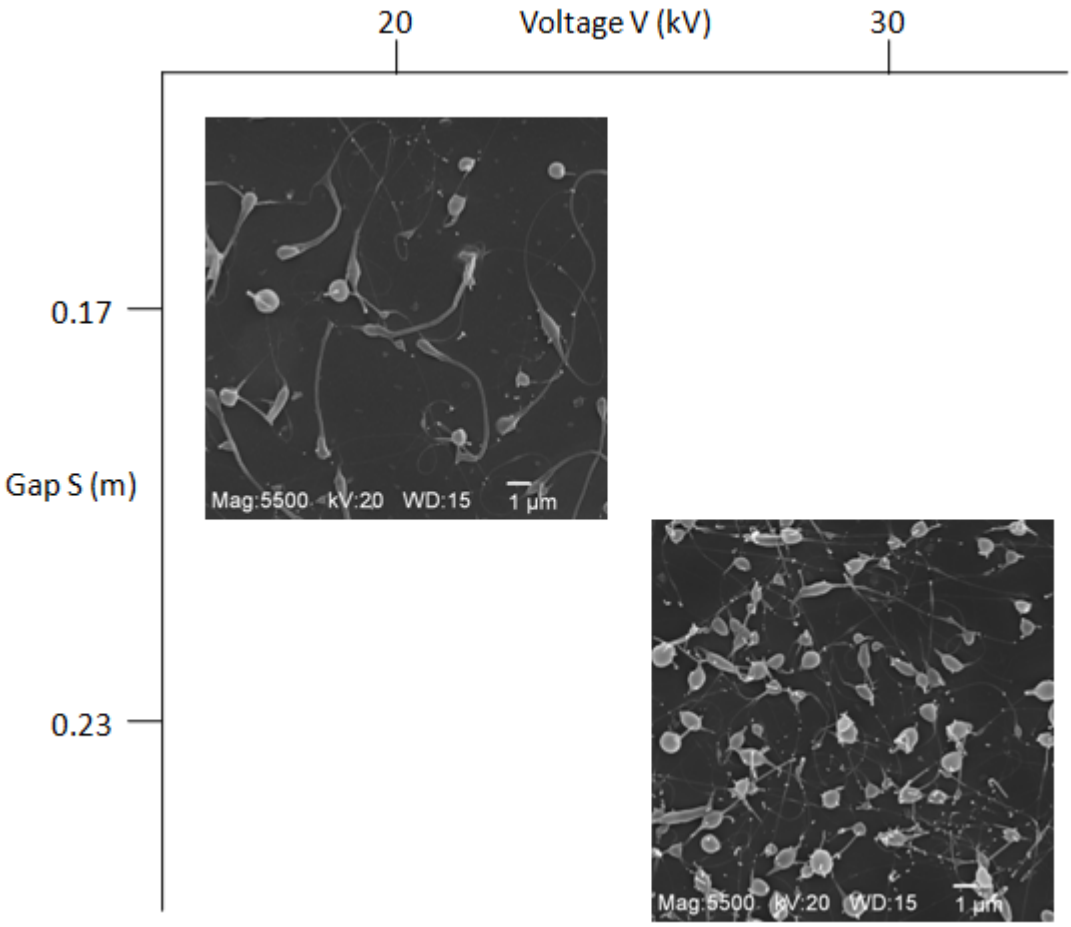

Figure 4.13 SEM images for polymer concentration of 1%w/v.

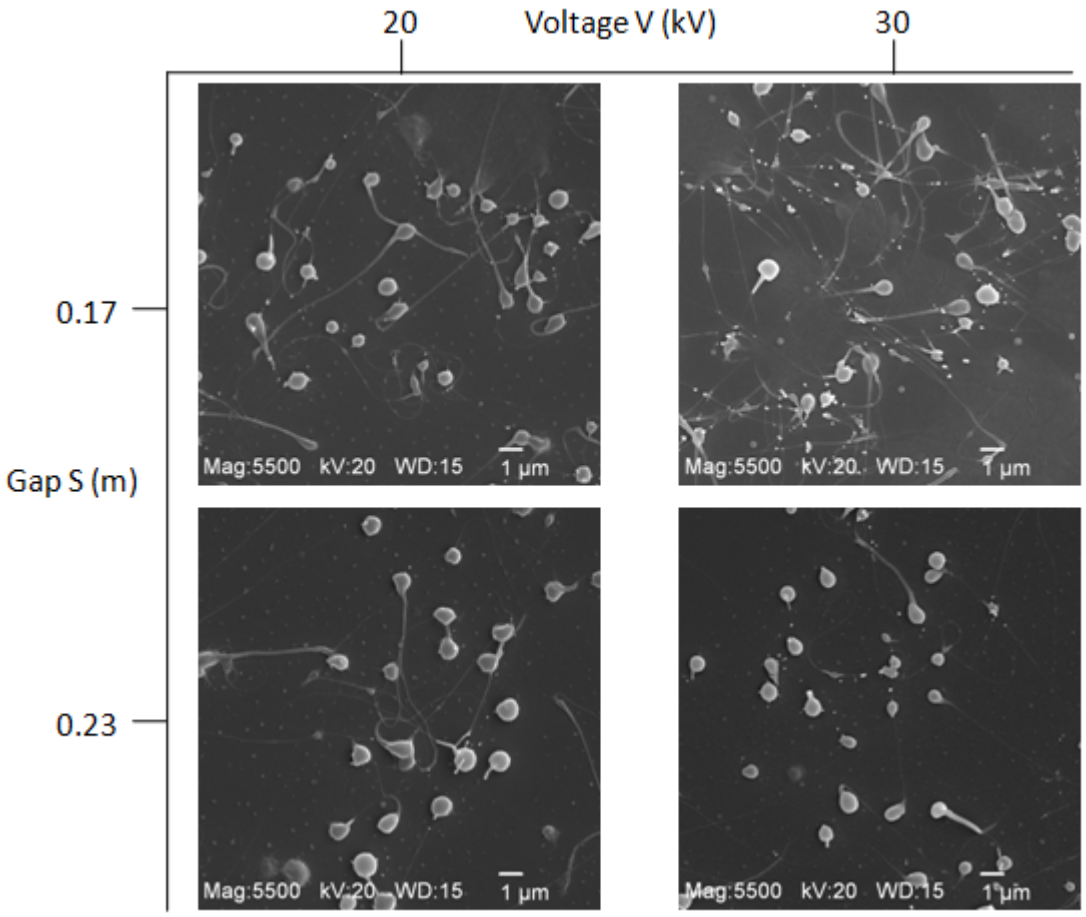

Figure 4.14 SEM images for polymer concentration of 0.5%w/v.

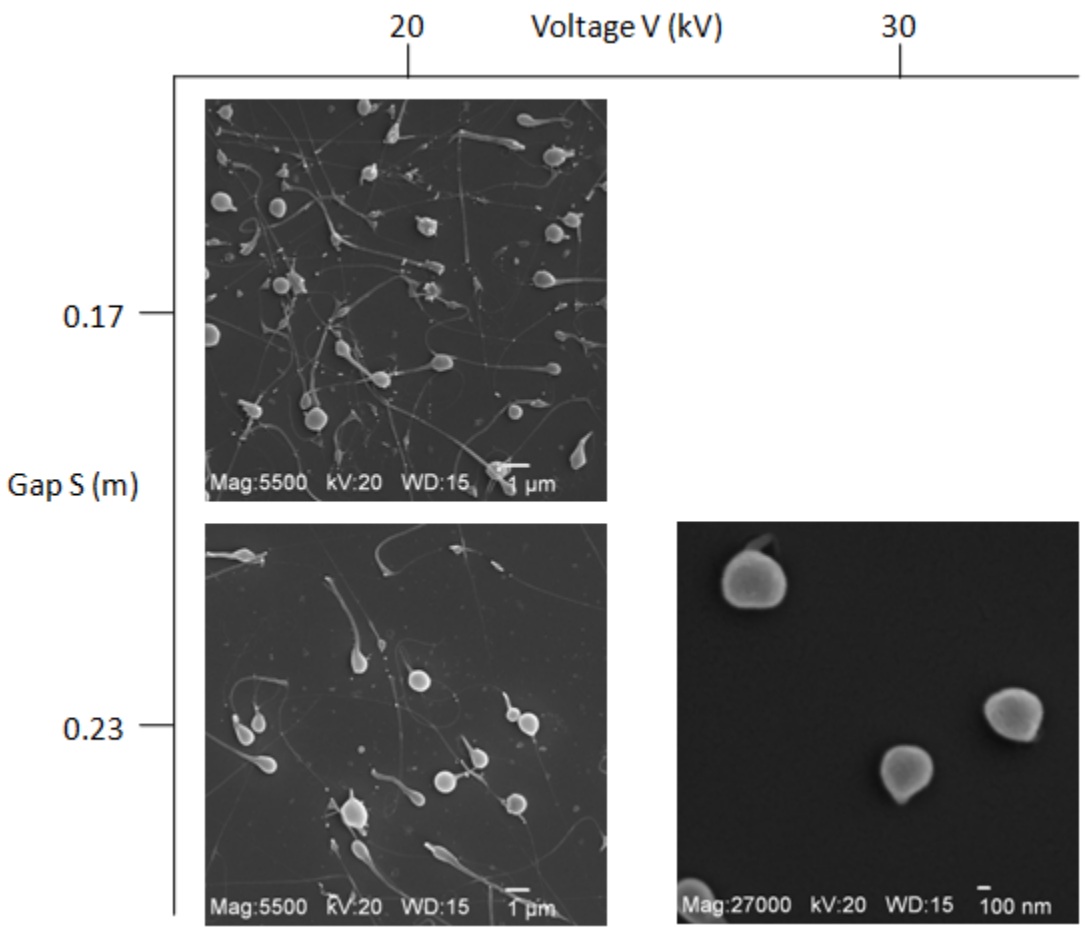

Figure 4.15 SEM images for polymer concentration of 0.25%w/v.

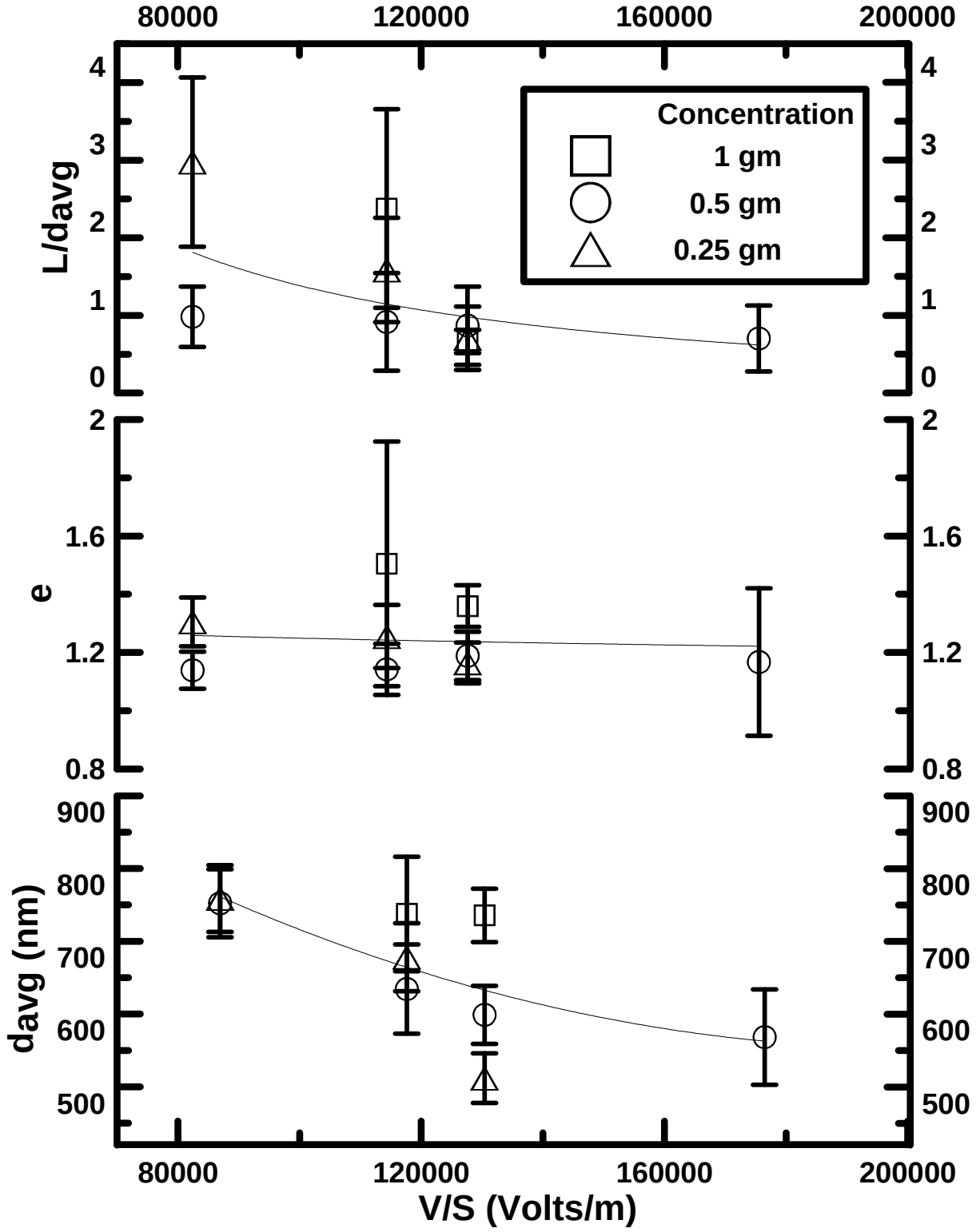

Figure 4.16 The L/d_{avg}, e and d_{avg} plotted against V/S.

CHAPTER V

CONCLUSION

5.1 Summary

This study showed that the morphology of the fibers produced by electrospinning of aqueous solutions of PEO at different concentrations is influenced by parameters such as the applied voltage, the distance between the nozzle tip and grounded electrode and the concentration of the solution. The formation of polymer spheres in sub-micron range was observed. The conditions at which beaded and non-beaded fibers formed was also illustrated.

5.2 Conclusions

Observations of electrospinning of aqueous solutions of PEO at different concentrations yielded the following major conclusions:

1. Digital holographic microscopy can be used to observe the trajectory of the electrospinning jet.
2. By making a few improvements, the change in morphology of the fiber as the jets propagates towards the collector can be inspected using digital holographic microscopy.
3. As the concentration of the solution decreases, beaded fibers are formed. Further reduction in the concentration results in the generation of beads with spindle-like structures. This could possibly be attributed to the decrease in the

viscosity of the polymer solution, and hence a decrease in the damping of the axis-symmetric disturbances along the jet surface.

4. Increasing the applied voltage and the traveling distance favors the formation of sphere-like structures with short tails.
5. Spheres of PEO were observed for the following test conditions: applied voltage = 30kV, gap = 0.23m and initial polymer concentration of 0.25% by weight.

5.3 Recommendations for future Studies

Based on the present experimental results for electrospinning of PEO, the following recommendations are made concerning future studies:

1. A theoretical model is required to achieve better control over the size and morphology of the electrospun fiber.
2. Extensive investigation of the relation between the operating parameters (applied voltage, gap distance, air humidity, viscosity and surface tension of the solution) and the morphology of the electrospun fibers is to be made.
3. This study needs to be extended to other polymers and a generalized theory applicable to a broad range of polymers should be developed.

REFERENCES

Arayanarakul K, Choktaweesap N, Aht-ong D, Meechaisue C, Supaphol P. "Effects of Poly(ethylene glycol), Inorganic Salt, Sodium Dodecyl Sulfate, and Solvent System on Electrospinning of Poly (ethylene oxide)". *Macromol. Mater. Eng*. 2006, 291, 581–591.

Ayutsede, J, Gandhi M, Sukigara S, Micklus M, Chen HE. and Ko F. (2005). "Regeneration of Bombyx mori silk by electrospinning. Part 3: characterization of electrospun nonwoven mat". Polymer 46, pp. 1625-1634.

Baumgarten PK. "Electrostatic spinning of acrylic microfibers". *J of Colloid and Interface Science* 1971; 36:71–9.

Bognitzki M, Hou H, Ishaque M, Frese T, Hellwig M, Schwarte C, et al. "Polymer, metal, and hybrid nano- and mesotubes by coating degradable polymer template fibers (TUFT process)". *Adv Mater* 2000;12(9):637–40.

Bognitzki M, Czado W, Frese T, Schaper A, Hellwig M, Steinhart M, et al. "Nanostructured fibers via electrospinning", *Adv Mater* 2001;13:70–2.

Buchko CJ, Chen LC, Shen Y, Martin DC. "Processing and microstructural characterization of porous biocompatible protein polymer thin films". *Polymer* 1999; 40:7397–407.

Buchko CJ, Slattery MJ, Kozloff KM, Martin DC. "Mechanical properties of biocompatible protein polymer thin films". *J Mat Res* 2000; 15(1):231–42.

Buchko CJ, Kozloff KM, Martin DC. "Surface characterization of porous, biocompatible protein polymer thin films". *Biomaterials* 2001; 22(11):1289–300.

Chen ZH, Foster MD, Zhou WS, Fong H, Reneker DH, Resendes R, et al. "Structure of poly (ferrocenyldimethylsilane) in electrospun nanofibers". *Macromolecules* 2001; 34(18):6156–8.

Choi JS, Lee SW, Jeong L, Bae SH, Min BC, Youk JH. and Park WH. (2004)." Effect of organosoluble salts on the nanofibrous structure of electrospun poly(3-hydroxybutyrate-co-3-hydroxyvalerate)". *International Journal of Biological Macromolecules*, 34, 4, pp. 249-256.

Chun I, Reneker DH, Fong H, Fang X, Deitzel J, Tan NB, et al. “Carbon nanofibers from polyacrylonitrile and mesophase pitch”. *Journal of Advanced Materials* 1999; 31(1):36–41.

Dai H-Q, Gong J, Kim H, Lee D. “A novel method for preparing ultra-fine alumina-borate oxide fibers via an electrospinning technique”. *Nanotechnology* 2002; 13(5):674–7.

Deitzel JM, Kleinmeyer J, Harris D, Tan NCB. “The effect of processing variables on the morphology of electrospun nanofibers and textiles”. *Polymer* 2001; 42:261–72.
Deitzel JM, Kleinmeyer J, Hirvonen JK, BeckTNC. “Controlled deposition of electrospun poly(ethylene oxide) fibers”. *Polymer* 2001; 42:8163–70.

Deitzel JM, KosikW, McKnight SH, Ten NCB, Desimone JM, Crette S. “Electrospinning of polymer nanofibers with specific surface chemistry”. *Polymer* 2002; 43(3):1025–9.

Demir MM, Yilgor I, Yilgor E, Erman B. “Electrospinning of polyurethane fibers”. *Polymer* 2002; 43:3303–9.

Doi M, 1996 “Introduction to Polymer Physics” (Oxford: Clarendon)

Doshi J, Reneker DH. “Electrospinning process and applications of electrospun fibers”. *J Electrostatics* 1995; 35(2-3):151–60.

Fang X, Reneker DH. “DNA fibers by electrospinning”. *J Macromolecular Sci-Phys* 1997; B36:169–73.

Fong H, Chun I, Reneker DH. “Beaded nanofibers formed during electrospinning”. *Polymer* 1999; 40:4585–92.

Fong H, Liu W-D, Wang C-S, Vaia RA. “Generation of electrospun fibers of nylon 6 and nylon 6-montmorillonite nanocomposite”. *Polymer* 2002; 43(3):775–80.

Gabor DA, New Microscopic Principle, Nature, vol. 161(4098), pp. 777-778, 1948.

Gibson PW, Schreuder-Gibson HL, Riven D. “Electrospun fiber mats: transport properties”. *AIChE J* 1999; 45(1):190–5.

Goodman JW and Lawrence RW, Digital Image Formation from Electronically Detected Holograms, 12 *Applied Physics Letters*, vol. 11(3), pp. 77-79, 1967.

Hohman MM, Shin M, Rutledge G, Brenner MP. “Electrospinning and electrically forced jets. I. Stability theory”. *Physics of Fluids* 2001; 13:2201–20.

Hohman MM, Shin M, Rutledge G, Brenner MP. “Electrospinning and electrically forced jets. II. Applications”. *Physics of Fluids* 2001; 13:2221–36.

Huang C, Chen S, Lai1 C, Reneker DH, et al. “Electrospun polymer nanofibres with small diameters”. *Nanotechnology* 17 (2006) 1558–1563.

Huang L, Apkarian RP, Chaikof EL. “High-Resolution analysis of engineered type I collagen nanofibers by electron microscopy”. *Scanning* 2001a; 23:372–5.

Huang L, Nagapudi K, Apkarian R, Chaikof EL. “Engineered collagen-PEO nanofibers and fabrics”. *J Biomater Sci Polym Edn* 2001b; 12(9):979–94.

Huang ZM, Zhang YZ, Kotakic M, Ramakrishna S. “A review on polymer nanofibers by electrospinning and their applications in nanocomposites”. *Composites Science and Technology* 63 (2003) 2223–2253.

Jaeger R, Schonherr H, Vancso J. “Chain packing in electrospun poly- (ethylene oxide) visualized by atomic force microscopy”. *Macromolecules* 1996;29(23):7634–7636.

Jaeger R, Bergshoef M, Batlle C, Schonherr H, Vancso J. “Electrospinning of ultra-thin polymer fibers”. *Macromolecular Symposium* 1998;127:141–150.

Jin HJ, Fridrikh S, Rutledge GC, Kaplan D. “Electrospinning Bombyx mori silkwith poly(ethylene oxide)”. *Abstracts of Papers American Chemical Society* 2002; 224(1–2):408.

Kenawy ER, Bowlin GL, Mansfield K, Layman J, Simpson DG, Sanders EH, et al. “Release of tetracycline hydrochloride from electrospun poly(ethylene-co-vinylacetate), poly(lactic acid), and a blend”. *Journal of Controlled Release* 2002; 81:57–64.

Kenawy E-R, Layman JM, Watkins JR, Bowlin GL, Matthews JA, Simpson DG, et al. “Electrospinning of poly (ethylene-covinyl alcohol) fibers”. *Biomaterials* 2003; 24:907–13.

Kim JR., Choi SW., Jo SM., Lee WS. and Kim BC. (2005). Characterization and Properties of P(VdF-HFP)-Based Fibrous Polymer Electrolyte Membrane Prepared by Electrospinning. *J. Electrochem*. Soc. 152, pp. A295-A300.

Kim J-S, Lee D-S. “Thermal properties of electrospun polyesters”. *Polymer J* 2000; 32(7):616–8.

Kim J-S, Reneker D. H. “Mechanical properties of composites using ultrafine electrospun fibers”. *Polymer Composites* 1999; 20(1):124–31.

Koombhongse S, Liu WX, Reneker DH. “Flat polymer ribbons and other shapes by electrospinning”. *J Polymer Sci: Part B: Polymer Physics* 2001; 39:2598–606.

Krishnappa RVN, Sung CM, Schreuder-Gibson H. “Electrospinning of Polycarbonates and their surface characterization using the SEM and TEM”. *Mat Res Soc Symp Proc* 2002; 702:U6.7.1–0U6.7.6.

Larrondo, Manley R., St J. “Electrostatic fiber spinning from polymer melts, I. and Experimental observations on fiber formation and properties”. *J Polymer Science: Polymer Physics Edition* 1981; 19:909–20.

Larrondo, Manley R., St J. “Electrostatic fiber spinning from polymer melts. II. Examination of the flow field in an electrically driven jet”. *J Polymer Sci: Polymer Physics Ed* 1981; 19:921–32.

Lee J, Miller B, and Sallam K. A. “Demonstration of Digital Holographic Diagnostics for the Breakup of Liquid Jets Using a Commercial-Grade CCD Sensor”. *Atom. Sprays*, to appear in 2009, Vol. 19, No. 5.

Lee K.H, Kim H.Y, Bang H.J, Jung Y.H, Lee S.G. “The change of bead morphology formed on electrospun polystyrene fibers”. *Polymer* 44 (2003), 4029–4034.

Leith EN and Upatniek J, Holograms: Their Properties and Uses, *Society of Photo-Optical Instrumentation Engineers Journal*, vol. 4(1), 1965.

Li D, Xia Y. “Electrospinning of Nanofibers”. *Adv Mater* 2004, 16, No. 14.

Li WJ, Laurencin CT, Caterson EJ, Tuan RS, Ko FK. “Electrospun nanofibrous structure: A novel scaffold for tissue engineering”. *J Biomed Mater Res* 2002; 60(4):613–21.

Lin T, Wang HX, Wang HM. and Wang XG. (2004). “The charge effect of cationic surfactants on the elimination of fibre beads in the electrospinning of polystyrene”. *Nanotechnology*. 15, pp. 1375-1381.

MacDiarmid AG, Ones Jr WE, Norris ID, Gao J, Johnson AT, Pinto NJ, et al. “Electrostatically-generated nanofibers of electronic polymers”. *Synthetic Metals* 2001; 119:27–30.

Matthews JA, WnekGE, Simpson DG, Bowlin GL. “Electrospinning of Collagen Nanofibers”. *Biomacromolecules* 2002; 3(2):232–8.

Megelski S, Stephens JS, Rabolt JF, Bruce CD. “Micro-and nanostructured surface morphology on electrospun polymer fibers”. *Macromolecules* 2002; 35(22):8456–66.

Mit-uppatham C, Nithitanakul M. and Supaphol P. (2004). “Ultrafme Electrospun Polyarnide-6 Fibers: Effect of Solution Conditions on Morphology and Average Fiber Diameter”. *Macromol. Chem*. Physic. 205, pp. 2327-2338.

Morozov VN, Morozova TY, Kallenbach NR. “Atomic force microscopy of structures produced by electrospraying polymer solutions. International” *Journal of Mass Spectrometry* 1998; 178:143–59.

Ondarcuhu T, Joachim C. “Drawing a single nanofibre over hundreds of microns”. *Europhys Lett* 1998; 42(2):215–20.

Reneker DH, Chun I. “Nanometre diameter fibres of polymer, produced by electrospinning”. *Nanotechnology* 1996; 7:216–23.

Reneker DH, Yarin AL, Fong H, Koombhongse S. “Bending instability of electrically charged liquid jets of polymer solutions in electrospinning”. *J Appl Phys* 2000; 87:4531–47.

Rutledge GC, Li Y, Fridrikh S, Warner SB, Kalayci VE. and Patra P. (2000). “Electrostatic Spinning and Properties of Ultrafine Fibers”, National Textile Center, 2000 Annual Report (M98-D01), National Textile Center, pp. 1-10

Schnars U and Juptner W, Direct Recording of Holograms by a CCD Target and Numerical Reconstruction, *Applied Optics*, vol. 33(2), pp. 179-181, 1994.

Schreuder-Gibson HL, Gibson P. “Transport properties of electrospun non woven membranes”. *Int Nonwoven J* 2002; 11(2):21–6.

Schreuder-Gibson HL, Gibson P, Senecal K, Sennett M, Walker J, Yeomans W, et al. “Protective textile materials based on electrospun nanofibers”. *Journal of Advanced Materials* 2002; 34(3):44–55.

Senador Jr AE, Shawa MT, Mathera PT. “Electrospinning of Polymeric Nanofibers: Analysis of Jet Formation”. *Mat Res Soc Symp Proc* 2001; 661:KK5.9.1–0KK5.9.

Shao CL, Kim H-Y, Gong J, Ding B, Lee D-R, ParkS-J. “Fiber mats of poly (vinyl alcohol)/silica composite via electrospinning”. *Materials Letters* 2002; 56(1-2):24–9.

Shin YM, Hohman MM, Brenner MP, Rutledge GC. “Electrospinning: A whipping fluid jet generates submicron polymer fibers”. *Appl Phys Lett* 2001; 78:1149–51.

Shin YM, Hohman MM, Brenner MP, Rutledge GC. “Experimental characterization of electrospinning: the electrically forced jet and instabilities”. *Polymer* 2001; 42:9955–67.

Son WK, Youk JH, Lee TS. and Park WH. (2004). “Electrospinning of ultrafine cellulose acetate fibers: studies of a new solvent system and deacetylation of ultrafme cellulose acetate fibers”, *J. Polym. Sci. Pt. B-Polym. Phys.* 42, pp. 5-11.

Srinivasan G, Reneker DH. “Structure and morphology of small diameter electrospun aramid fibers”. *Polym Int* 1995; 36(2):195–201.

Taylor GI. “Disintegration of water drops in an electric field”. *Proc R Soc London*, Ser A 1964; 280:383.

Taylor GI. “The circulation produced in a drop by an electric field”. *Proc R Soc London*, Ser A 1966; 291:159.

Taylor GI. “Electrically driven jets”. *Proc R Soc London*, Ser A 1969; 313:453–75.

Theron A, Zussman E, Yarin AL. “Electrostatic field-assisted alignment of electrospun nanofibers”. *Nanotechnology* 2001; 12:384–90.

Tsaia PP, Schreuder-Gibson H, Gibson P. “Different electrostatic methods for making electret filters”. *Journal of Electrostatics* 2002; 54:333–41.

Vonnegut B, Neubauer RL. *J of Colloid Science* 1952; 7:616.

Wang Y, Serrano S, Santiago-Aviles JJ. “Conductivity measurement of electrospun PAN-based carbon nanofibers”. *Journal of Materials Science Letters* 2002; 21(13):1055–7.

Wannatong L, Sirivat A. and Supaphol P. (2004). “Effects of solvents on electrospun polymeric fibers: preliminary study on polystyrene”. *Polym. Int*. 53, 1851-1859.

Warner SB, Buer A, Grimler M, Ugbolue SC, Rutledge GC, Shin MY. “A fundamental investigation of the formation and properties of electrospun fibers”. In: 1999 Annual Report (M98-D01), National Textile Center, 1999.

Warner SB, Buer A, Grimler M, Ugbolue SC, Rutledge GC, Shin MY. “A fundamental investigation of the formation and properties of electrospun fibers”. In: 2001 Annual Report (M98-D01), National Textile Center, 2001.

Yarin AL, Koombhongse S, Reneker DH. “Bending instability in electrospinning of nanofibers”. *J Appl Phys* 2001;89(5):3018–26.

Yarin AL, Koombhongse S, Reneker DH. “Taylor cone and jetting from liquid droplets in electrospinning of nanofibers”. *J Appl Phys* 2001;89(9):4836–46.

Zeng J., Xu X., Chen X., Liang Q., Bian X., Yang L. and ling X. (2003). Biodegradable electrospun fibers for drug delivery, *J. Control.* Release, 92, pp. 227-231.

Zhang W, Huang Z, Yan E et al. “Preparation of poly(phenylene vinylene) nanofibers by electrospinning”. *Materials Science and Engineering* A 443 (2007) 292–295.

Zhao SL., Wu XH., Wang LG. and Huang Y. (2004). Electrospinning of Ethyl-Cyanoethyl Cellulose/Tetrahydrofuran Solutions. *J. Appl. Polym. Sci*. 91, pp. 242- 246.

Zhong XH, Kim KS, Fang DF, Ran SF, Hsiao BS. and Chu B. (2002). Structure and process relationship of Electrospun bioabsorbable nanofiber membranes. *Polymer*. 43, pp. 4403-4412.

Zong X, Kim K, Fang D, Ran S, Hsiao BS, Chu B. "Structure and process relationship of electrospun bioabsorbable nanofiber membranes". *Polymer* 2002; 43(16):4403–12.

Zuo W, Zhu M, Yang W, Yu H, Chen Y, Zhang Y. "Experimental Study on Relationship Between Jet Instability and Formation of Beaded Fibers During Electrospinning". *Polymer Engineering and Science* 2005. 45:704-709.

APPENDIX

EXPERIMENTAL DATA

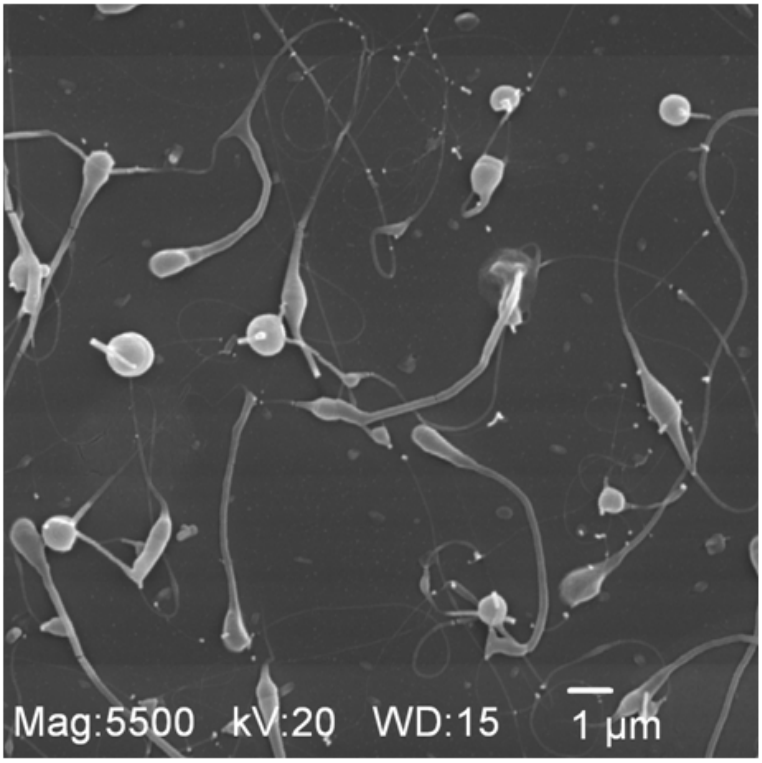

Figure A.1 SEM image obtained for concentration=1%w/v, Gap=0.17m, Voltage=20kV.

S.No	dmax (nm)	dmin (nm)	Tail Length L(nm)	Avg Dia d_{avg}(nm)	dmax/dmin e	L/d_{avg}	V/S (V/m)
1	690.3351	672.601352	438.6147	681.4105	1.026366	0.6436864	117647.06
2	971.3926	906.384688	399.2791	938.3258	1.071722	0.4255229	117647.06
3	883.8835	657.179401	710.2476	762.1483	1.344965	0.9319021	117647.06
4	881.8094	824.579675	203.7251	852.7146	1.069405	0.2389136	117647.06
5	826.3542	528.716385	3971.709	660.9894	1.562944	6.0087323	117647.06
6	777.6479	696.145919	1683.009	735.7693	1.117076	2.2874141	117647.06
7	828.7144	484.375	4563.322	633.5681	1.710894	7.202575	117647.06
8	530.5602	524.078432	1319.817	527.3094	1.012368	2.5029275	117647.06
9	1447.654	444.14595	4737.93	801.854	3.259411	5.9087191	117647.06
10	1202.212	572.182294	1840.37	829.3878	2.101099	2.2189503	117647.06
11	657.1794	524.078432	963.66	586.8676	1.253971	1.64204	117647.06
12	697.5473	576.221529	3714.717	633.9888	1.210554	5.8592795	117647.06

Table A.1 Measurements made from SEM image in Fig. A.1.

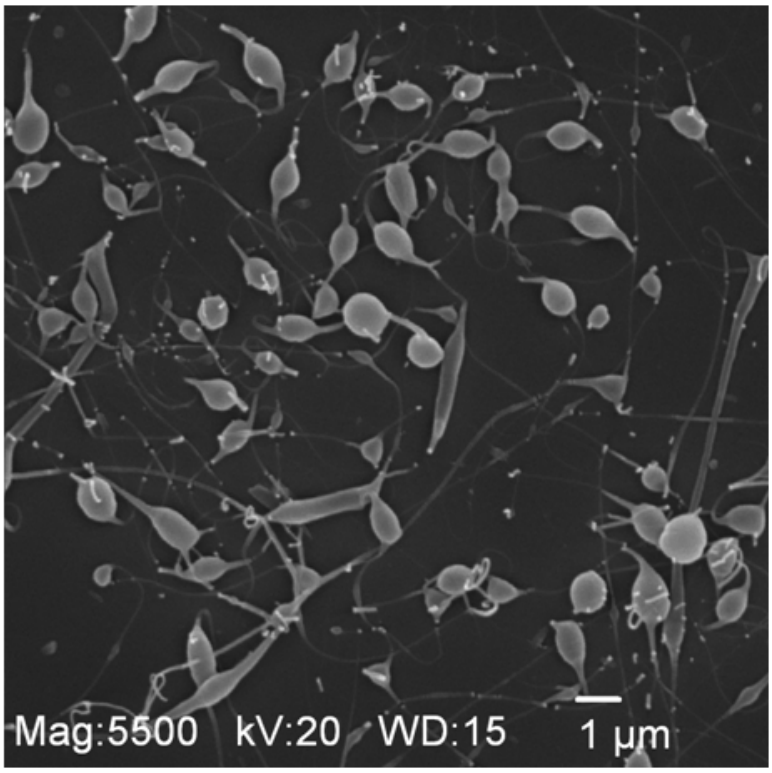

Figure A.2 SEM image obtained for concentration=1%w/v, Gap=0.23m, Voltage=30kV.

S.No	dmax	dmin	Tail Length	Avg Dia	dmax/dmin	L/d_{avg}	V/S
	(nm)	(nm)	L(nm)	d_{avg}(nm)	e		(V/m)
1	927.1798	612.500996	562.9888	753.5904	1.51376	0.7470753	130434.78
2	1179.847	676.793829	604.4264	893.5955	1.743288	0.6763982	130434.78
3	918.5801	607.544737	305.3236	747.0465	1.511955	0.4087076	130434.78
4	1083.559	766.027207	1081.231	911.0628	1.414517	1.1867798	130434.78
5	794.2855	588.158962	1111.442	683.4955	1.350461	1.6261141	130434.78
6	756.0956	568.99836	714.9908	655.9094	1.328819	1.0900756	130434.78
7	857.1429	634.920635	381.6132	737.7111	1.35	0.5172935	130434.78
8	874.3136	616.396439	924.0848	734.1143	1.418427	1.2587751	130434.78
9	958.8405	585.367902	597.7197	749.1825	1.638014	0.7978292	130434.78
10	952.381	683.277563	1222.487	806.6849	1.393842	1.5154451	130434.78
11	827.8352	632.535201	435.8581	723.6262	1.308758	0.6023249	130434.78
12	998.9917	666.855604	892.636	816.2005	1.498063	1.093648	130434.78
13	830.5699	630.140738	587.516	723.4472	1.31807	0.8121063	130434.78
14	730.3312	650.793651	222.2222	689.4164	1.122216	0.3223338	130434.78
15	943.0762	747.212844	348.4841	839.4514	1.262125	0.4151331	130434.78
16	928.9444	642.80815	602.3386	772.7438	1.445135	0.7794803	130434.78
17	819.2691	540.61544	639.9654	665.5145	1.515438	0.9616101	130434.78

Table A.2 Measurements made from SEM image in Fig. A.2.

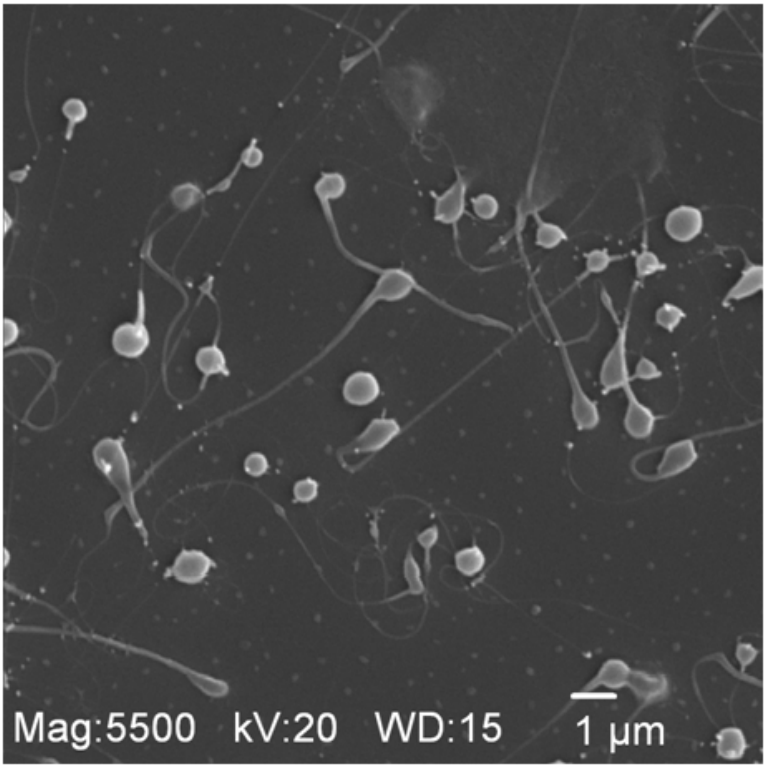

Figure A.3 SEM image obtained for concentration=0.5%w/v, Gap=0.17m, Voltage=20kV.

S.No	dmax	dmin	Tail Length	Avg Dia	dmax/dmin	L/d_{avg}	V/S
	(nm)	(nm)	L(nm)	d_{avg}(nm)	e		(V/m)
1	1002.014	752.086206	823.2573	868.1017	1.332312	0.948342	117647.06
2	730.3312	642.023759	475.6611	684.7554	1.137546	0.6946437	117647.06
3	853.313	516.787955	501.1953	664.0647	1.651186	0.7547388	117647.06
4	778.4254	773.066391	369.1969	775.7413	1.006932	0.4759279	117647.06
5	551.0017	482.758931	247.9444	515.7529	1.14136	0.4807427	117647.06
6	439.0259	286.154863	123.9722	354.4424	1.534225	0.3497669	117647.06
7	781.6554	600.872801	333.711	685.3287	1.300867	0.4869357	117647.06
8	869.5458	673.809056	772.4143	765.4462	1.290493	1.0091034	117647.06
9	853.313	740.438336	596.4538	794.8746	1.152443	0.7503747	117647.06
10	571.649	554.420609	392.6767	562.9689	1.031075	0.6975105	117647.06
11	651.3741	537.108708	2177.3	591.4886	1.212742	3.6810519	117647.06
12	562.5411	529.787913	356.7017	545.9189	1.061823	0.6533968	117647.06
13	762.731	762.731033	748.7287	762.731	1	0.9816418	117647.06
14	628.9401	581.321526	369.1969	604.6622	1.081914	0.6105838	117647.06
15	741.1186	669.683273	6742.297	704.4961	1.10667	9.5703831	117647.06
16	710.7496	573.409266	3389.672	638.3968	1.239515	5.3096638	117647.06
17	719.207	639.861726	2609.787	678.3753	1.124004	3.8471139	117647.06

Table A.3 Measurements made from SEM image in Fig. A.3.

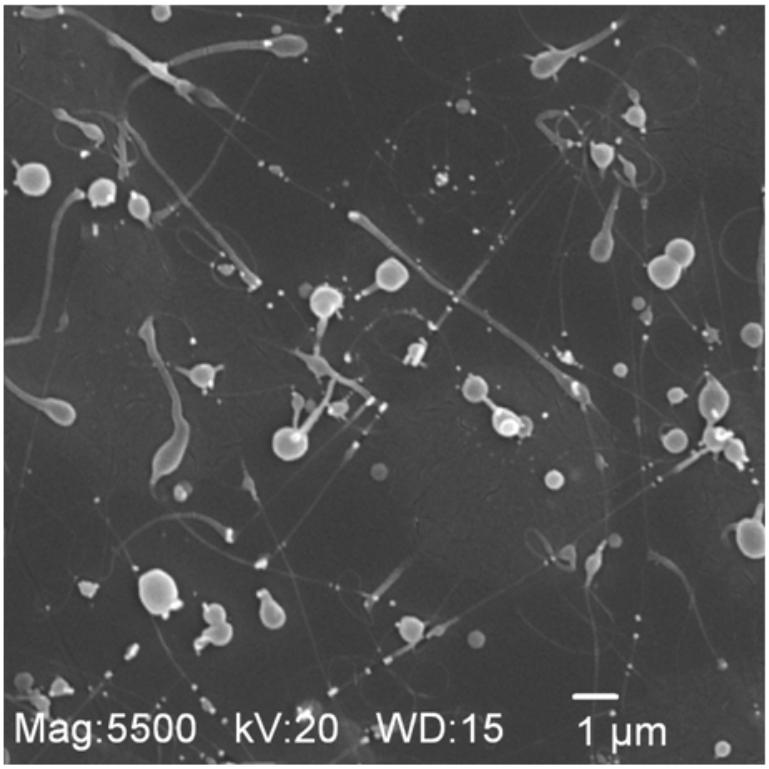

Figure A.4 SEM image obtained for concentration=0.5%w/v, Gap=0.17m, Voltage=30kV.

S.No	dmax	dmin	Tail Length	Avg Dia	dmax/dmin	L/d_{avg}	V/S
	(nm)	(nm)	L(nm)	d_{avg}(nm)	e		(V/m)
1	888.4293	475.215823	1126.085	649.7659	1.869528	1.7330621	176470.59
2	516.5711	455.543117	244.5699	485.0984	1.133968	0.5041657	176470.59
3	803.435	521.509977	2377.153	647.3016	1.540594	3.6724034	176470.59
4	676.2214	632.18526	377.5952	653.8327	1.069657	0.5775104	176470.59
5	716.8794	681.257167	1230.774	698.8413	1.052289	1.7611641	176470.59
6	703.125	625.780762	850.0919	663.3265	1.123596	1.2815587	176470.59
7	609.375	474.444577	977.9053	537.6938	1.284397	1.8187029	176470.59

Table A.4 Measurements made from SEM image in Fig. A.4.

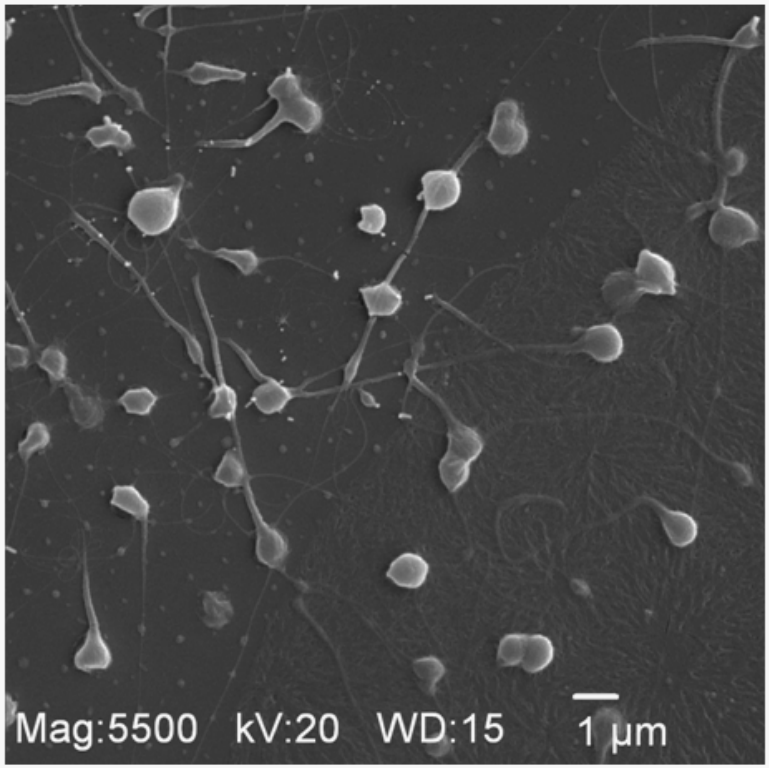

Figure A.5 SEM image obtained for concentration=0.5%w/v, Gap=0.23m, Voltage=20kV.

S.No	dmax	dmin	Tail Length	Avg Dia	dmax/dmin	L/d_{avg}	V/S
	(nm)	(nm)	L(nm)	d_{avg}(nm)	e		(V/m)
1	1057.548	935.022769	557.9147	994.4001	1.13104	0.5610565	86956.522
2	831.802	765.625	1077.219	798.0278	1.086435	1.3498512	86956.522
3	752.5997	682.510302	732.3776	716.6987	1.102693	1.0218766	86956.522
4	822.0592	678.384167	998.2896	746.7743	1.21179	1.3368022	86956.522
5	805.4077	662.175628	2231.635	730.2886	1.216305	3.0558258	86956.522
6	831.802	801.000351	3500.679	816.2559	1.038454	4.2887029	86956.522
7	705.0321	610.175756	1975.687	655.8914	1.155457	3.0122168	86956.522
8	830.4801	662.918217	1728.368	741.9841	1.252764	2.3293863	86956.522
9	816.2474	734.541205	539.6849	774.3173	1.111234	0.6969815	86956.522
10	868.4183	761.949084	560.9788	813.4436	1.139733	0.6896346	86956.522
11	781.8748	656.435986	2608.352	716.4152	1.191091	3.6408379	86956.522
12	830.4801	822.059152	606.4279	826.2589	1.010244	0.7339442	86956.522
13	911.0862	844.328505	1042.501	877.0724	1.079066	1.1886142	86956.522
14	806.6193	546.65174	278.1952	664.033	1.475563	0.4189479	86956.522
15	884.1596	664.384113	866.7535	766.4344	1.330796	1.1308907	86956.522
16	940.7496	923.065968	748.2075	931.8658	1.019157	0.8029133	86956.522

Table A.5 Measurements made from SEM image in Fig. A.5.

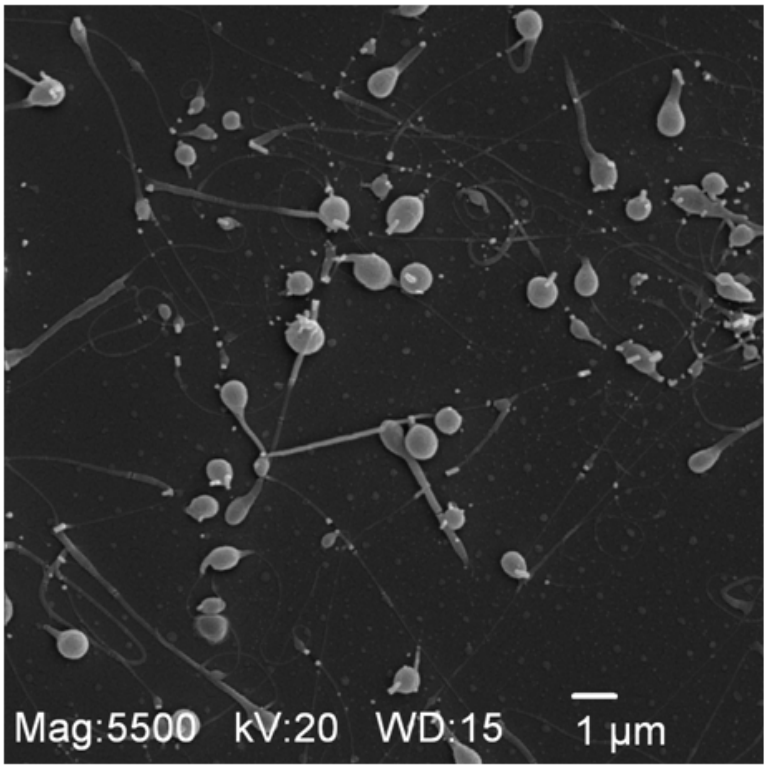

Figure A.6 SEM image obtained for concentration=0.5%w/v, Gap=0.23m, Voltage=30kV.

S.No	dmax	dmin	Tail Length	Avg Dia	dmax/dmin	L/d_{avg}	V/S
	(nm)	(nm)	L(nm)	d_{avg}(nm)	e		(V/m)
1	641.3867	609.375	337.2974	625.176	1.052532	0.5395239	130434.78
2	853.5313	623.827024	3662.983	729.6957	1.368218	5.0198771	130434.78
3	641.3867	578.125	376.2998	608.9349	1.109426	0.617964	130434.78
4	432.1661	298.515206	359.375	359.1771	1.447719	1.0005511	130434.78
5	532.1683	519.399067	5426.78	525.7449	1.024585	10.322078	130434.78
6	727.0244	667.500293	306.9825	696.6269	1.089175	0.44067	130434.78
7	734.375	671.147862	247.9304	702.05	1.094207	0.3531521	130434.78
8	859.375	512.538108	3416.784	663.6734	1.676705	5.1482911	130434.78
9	657.922	553.751411	234.375	603.5936	1.188118	0.3882994	130434.78
10	692.1011	586.510137	1501.248	637.1219	1.180033	2.3562964	130434.78
11	539.4586	499.267041	681.5703	518.9739	1.080501	1.3133036	130434.78
12	603.1331	603.133096	459.8106	603.1331	1	0.76237	130434.78
13	730.5419	528.716385	806.6193	621.4897	1.381727	1.2978805	130434.78
14	629.8639	554.852528	1827.897	591.1697	1.135192	3.0920009	130434.78
15	806.6193	594.982274	633.15	692.7656	1.355703	0.9139454	130434.78
16	791.1868	603.133096	1975.691	690.7901	1.311795	2.8600456	130434.78
17	687.6775	578.125	919.0901	630.5264	1.189496	1.4576551	130434.78
18	629.0882	595.597455	312.5	612.1138	1.05623	0.510526	130434.78
19	620.2948	512.538108	425.3055	563.8481	1.210241	0.7542909	130434.78

Table A.6 Measurements made from SEM image in Fig. A.6.

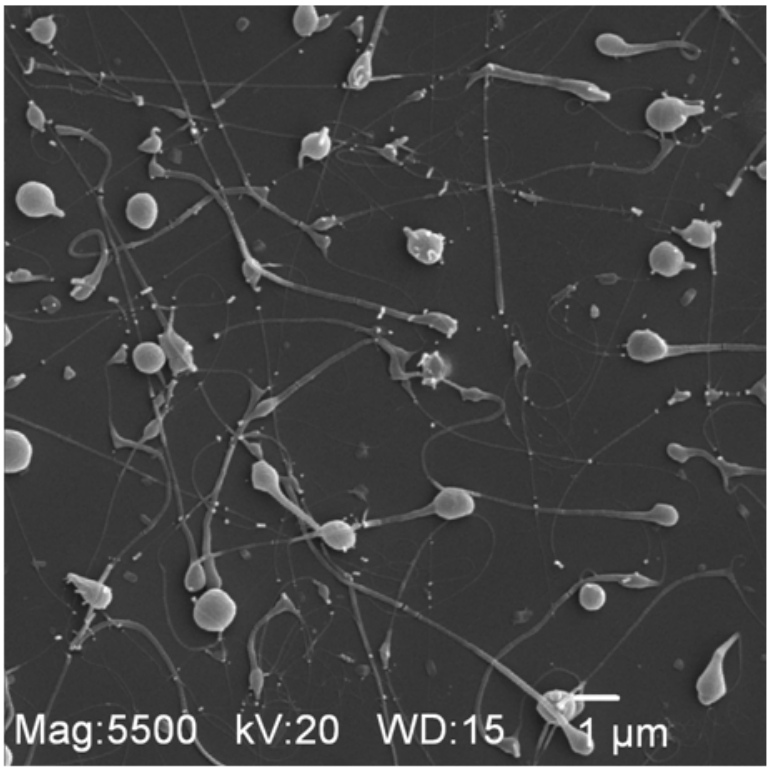

Figure A.7 SEM image obtained for concentration=0.25%w/v, Gap=0.17m, Voltage=20kV.

S.No	dmax	dmin	Tail Length	Avg Dia	dmax/dmin	L/d_{avg}	V/S
	(nm)	(nm)	L(nm)	d_{avg}(nm)	e		(V/m)
1	682.7242	539.915916	354.9314	607.1356	1.264501	0.5845999	117647.06
2	817.1135	783.586987	494.3623	800.1747	1.042786	0.6178179	117647.06
3	754.5946	483.54115	4887.185	604.0509	1.560559	8.0906836	117647.06
4	730.8485	471.93869	1988.458	587.2952	1.548609	3.3857889	117647.06
5	909.7606	606.507085	315.0704	742.8164	1.5	0.4241564	117647.06
6	947.3412	717.804384	415.4366	824.6245	1.319776	0.5037888	117647.06
7	875.4655	663.066621	303.2535	761.9002	1.320328	0.3980226	117647.06
8	873.0159	681.801003	6524.008	771.507	1.280456	8.4561872	117647.06
9	924.4584	689.15217	1122.186	798.1808	1.341443	1.4059296	117647.06
10	864.3145	816.187945	339.3263	839.9066	1.058965	0.4040048	117647.06
11	868.386	673.622069	3872.912	764.8294	1.289129	5.06376	117647.06
12	657.7254	605.051383	2488.66	630.8388	1.087057	3.9450018	117647.06
13	874.3136	825.549436	3311.714	849.5817	1.059069	3.8980528	117647.06
14	619.0476	539.68254	644.5695	578.0045	1.147059	1.1151636	117647.06
15	863.8771	419.059644	533.5789	601.6777	2.061466	0.8868185	117647.06
16	781.8165	746.706888	264.1796	764.0601	1.047019	0.3457577	117647.06
17	602.3386	588.158962	269.8413	595.2066	1.024109	0.4533574	117647.06
18	537.1087	533.578931	2392.412	535.3409	1.006615	4.4689504	117647.06
19	841.8686	666.855604	1239.011	749.2695	1.262445	1.6536248	117647.06
20	775.0194	650.793651	1531.169	710.1955	1.190883	2.1559827	117647.06
21	508.1845	485.620906	3607.852	496.7746	1.046463	7.2625537	117647.06
22	634.9206	559.171903	1333.711	595.8438	1.135466	2.2383573	117647.06
23	1097.192	647.689072	1143.056	842.9941	1.69401	1.3559472	117647.06
24	658.4911	427.394032	2622.199	530.5046	1.540712	4.9428398	117647.06
25	743.8333	413.917613	6623.443	554.8745	1.797056	11.936831	117647.06

Table A.7 Measurements made from SEM image in Fig. A.7.

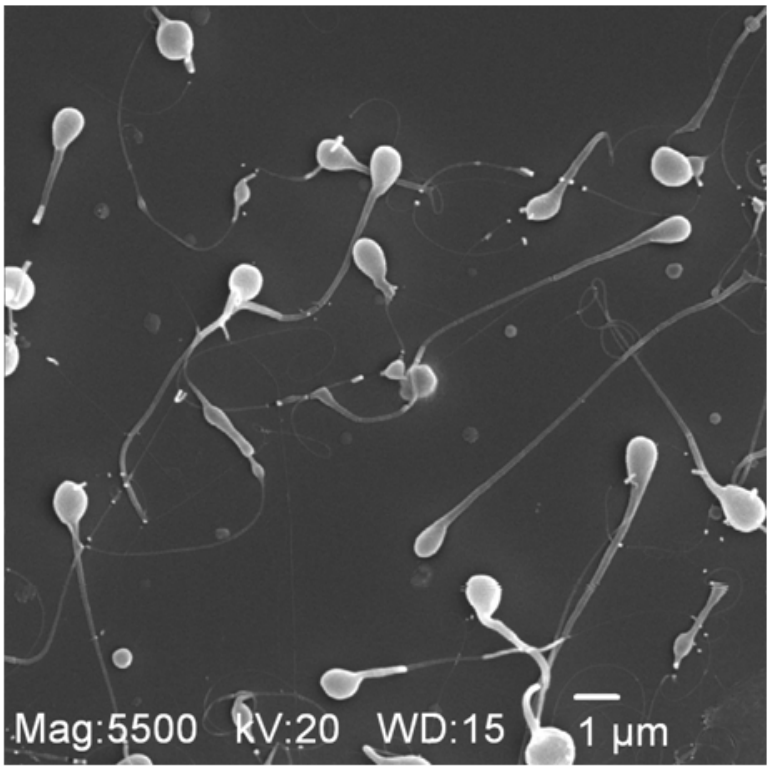

Figure A.8 SEM image obtained for concentration=0.25%w/v, Gap=0.23m, Voltage=20kV.

S.No	dmax	dmin	Tail Length	Avg Dia	dmax/dmin	L/d_{avg}	V/S
	(nm)	(nm)	L(nm)	d_{avg}(nm)	e		(V/m)
1	958.8405	632.535201	1744.109	778.7813	1.515869	2.2395357	86956.522
2	1049.541	683.277563	3460.114	846.8341	1.536039	4.0859413	86956.522
3	918.5801	637.494782	295.2552	765.2385	1.440922	0.3858342	86956.522
4	752.7559	692.980316	1762.191	722.25	1.086259	2.4398626	86956.522
5	823.2573	550.315423	1844.964	673.0908	1.495974	2.7410333	86956.522
6	858.4646	524.049969	7290.791	670.7297	1.638135	10.869939	86956.522
7	809.3682	698.59305	5737.509	751.9435	1.158569	7.6302403	86956.522
8	1003.144	734.459384	4596.173	858.3524	1.365827	5.3546461	86956.522
9	892.4249	495.888868	8759.309	665.2395	1.799647	13.167151	86956.522
10	1090.974	693.343799	3658.961	869.7241	1.573496	4.2070365	86956.522
11	1069.163	876.615954	3501.963	968.1142	1.219648	3.617303	86956.522
12	813.7146	689.882978	900.2953	749.2449	1.179497	1.2016035	86956.522
13	968.7743	762.565851	915.6956	859.5081	1.270414	1.0653717	86956.522
14	848.5756	650.987195	3237.661	743.2442	1.303521	4.3561203	86956.522
15	862.4176	841.86861	1104.543	852.0812	1.024409	1.2962889	86956.522
16	728.4314	582.13082	558.27	651.1853	1.251319	0.8573135	86956.522
17	839.471	647.689072	628.9401	737.3711	1.296102	0.8529492	86956.522
18	832.9931	669.683273	2224.772	746.8879	1.243861	2.9787224	86956.522
19	587.516	587.301587	713.5644	587.4088	1.000365	1.2147663	86956.522
20	947.0752	808.277908	2938.956	874.9285	1.17172	3.3590811	86956.522
21	788.0757	657.725376	708.7973	719.9565	1.198183	0.9845001	86956.522
22	902.95	866.498036	535.4644	884.5363	1.042068	0.6053617	86956.522
23	841.8686	730.331243	325.6871	784.1192	1.152722	0.415354	86956.522
24	704.5188	482.758931	1911.371	583.1918	1.459359	3.2774305	86956.522
25	1219.746	968.774255	336.7175	1087.041	1.259061	0.309756	86956.522
26	843.513	546.640488	4351.69	679.0422	1.543086	6.408571	86956.522
27	910.8677	506.19742	5441.987	679.0279	1.799432	8.0143792	86956.522
28	610.8534	525.969572	1199.451	566.8247	1.161385	2.1160882	86956.522

Table A.8 Measurements made from SEM image in Fig. A.8.

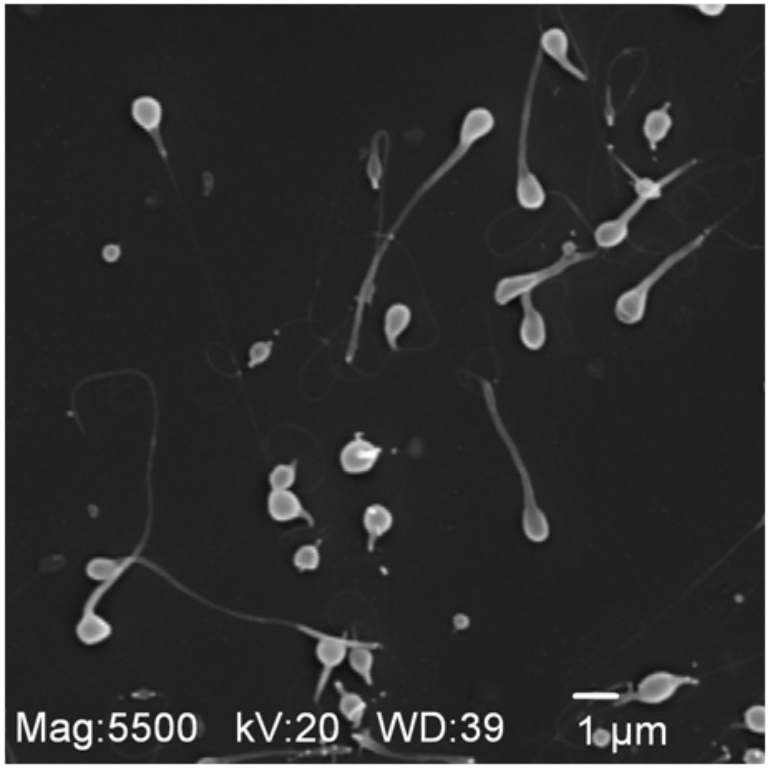

Figure A.9 SEM image obtained for concentration=0.25%w/v, Gap=0.23m, Voltage=30kV.

S.No	dmax	dmin	Tail Length	Avg Dia	dmax/dmin	L/d_{avg}	V/S
	(nm)	(nm)	L(nm)	d_{avg}(nm)	e		(V/m)
1	778.4254	658.491064	667.6108	715.9512	1.182135	0.9324809	130434.78
2	399.6723	392.676726	0	396.1591	1.017815	0	130434.78
3	669.8714	532.160464	175.3232	597.0587	1.258777	0.2936448	130434.78
4	669.8714	517.031666	684.7509	588.5106	1.29561	1.1635321	130434.78
5	673.8091	627.937792	2822.64	650.4692	1.073051	4.3393905	130434.78
6	866.498	604.426437	5197.716	723.6949	1.433587	7.1821926	130434.78
7	712.8734	492.319442	215.8964	592.42	1.44799	0.3644313	130434.78
8	664.5848	550.086459	1986.166	604.6314	1.208146	3.2849198	130434.78
9	778.4254	633.729041	1673.395	702.3609	1.228325	2.3825286	130434.78
10	1012.892	460.31746	807.9365	682.8265	2.200422	1.1832236	130434.78
11	485.8802	439.025927	0	461.8593	1.106723	0	130434.78
12	532.3971	492.830943	0	512.2322	1.080284	0	130434.78
13	673.6221	647.883544	0	660.6275	1.039727	0	130434.78
14	691.5245	605.051383	0	646.8445	1.142919	0	130434.78
15	694.2517	594.973486	319.0437	642.6985	1.166862	0.4964127	130434.78
16	480.4046	477.247504	0	478.8235	1.006615	0	130434.78
17	699.1338	523.809524	2654.519	605.1553	1.33471	4.3865089	130434.78
18	832.8419	537.108708	528.7811	668.8248	1.550602	0.7906122	130434.78
19	746.0317	593.064816	8102.793	665.1655	1.257926	12.181618	130434.78
20	520.6736	515.078754	0	517.8686	1.010862	0	130434.78
21	604.4264	585.367902	0	594.8208	1.032558	0	130434.78
22	535.4644	477.511395	0	505.6583	1.121365	0	130434.78
23	802.6474	554.420609	498.4228	667.0864	1.447723	0.7471638	130434.78
24	366.457	312.662152	0	338.4926	1.172054	0	130434.78
25	671.3742	525.969572	0	594.241	1.276451	0	130434.78
26	717.2777	647.689072	0	681.5959	1.107441	0	130434.78
27	604.4264	492.830943	1400.608	545.7839	1.226438	2.5662321	130434.78
28	401.5591	373.606422	0	387.3307	1.074818	0	130434.78
29	636.7038	557.592637	506.1974	595.8367	1.14188	0.8495573	130434.78
30	508.3105	476.190476	0	491.9884	1.067452	0	130434.78
31	555.3288	349.206349	1146.819	440.3684	1.59026	2.6042253	130434.78
32	457.8478	396.825397	264.1796	426.246	1.153776	0.6197821	130434.78

S.No	dmax	dmin	Tail Length	Avg Dia	dmax/dmin	L/d_{avg}	V/S
	(nm)	(nm)	L(nm)	d_{avg}(nm)	e		(V/m)
33	493.0865	235.969345	1925.947	341.106	2.089621	5.6461845	130434.78
34	588.159	571.648987	0	579.8452	1.028881	0	130434.78
35	777.7778	730.848535	0	753.9481	1.064212	0	130434.78
36	428.8653	428.865273	0	428.8653	1	0	130434.78
37	457.8265	406.162357	0	431.2214	1.127201	0	130434.78
38	453.0176	409.707728	0	430.8188	1.105709	0	130434.78
39	491.2083	449.068007	288.9069	469.6658	1.093839	0.6151329	130434.78
40	535.7671	502.866443	138.7107	519.0562	1.065426	0.2672365	130434.78
41	655.3856	559.787176	0	605.7033	1.170776	0	130434.78
42	642.9306	576.303416	318.7474	608.7061	1.115611	0.5236474	130434.78
43	237.3737	227.272727	0	232.2683	1.044444	0	130434.78
44	585.9457	585.880355	0	585.913	1.000111	0	130434.78
45	464.6465	439.510028	762.2248	451.9035	1.057192	1.6866981	130434.78
46	601.0313	550.528217	0	575.2258	1.091736	0	130434.78
47	290.1734	208.788148	0	246.1397	1.389798	0	130434.78

Table A.9 Measurements made from SEM image in Fig. A.9.

VITA

Atul Narasimhan

Candidate for the Degree of

Master of Science

Thesis: FORMATION OF BIODEGRADABLE FIBERS AND SPHERES BY ELECTROSPINNING OF PEO SOLUTION.

Major Field: Mechanical Engineering

Biographical:

Personal Data:
Born in India, January 20 1985, the son of S.L.Narasimhan and L.N.Shobhana.

Education:
Completed the requirements for the Master of Science degree in Mechanical Engineering at Oklahoma State University, Stillwater, Oklahoma in December, 2008.

Experience:
Employed by Oklahoma State University, Department of Mechanical and Aerospace Engineering as a graduate teaching assistant, 2007 to 2008.

ADVISER'S APPROVAL: Dr. K.A.Sallam

Name: Atul Narasimhan Date of Degree: May, 2009

Institution: Oklahoma State University Location: Stillwater, Oklahoma

Title of Study: FORMATION OF BIODEGRADABLE FIBERS AND SPHERES BY ELECTROSPINNING OF PEO SOLUTION

Pages in Study: 87 Candidate for the Degree of Master of Science

Major Field: Mechanical Engineering

Scope and Method of Study:

An experimental process for obtaining fibers and spheres using electrospinning of a polymer (Polyethylene Oxide) solution in water were studied. The objectives of the study were to complete measurements of size of the generated fibers and spheres to develop phenomenological analyses to help interpret and correlate the measurements of the instability growth on the electrospun micro liquid (polymeric solution) jets. Digital holographic microscopy was used to observe the trajectory of the electrospun jet and the growth of instability on the electrospun micro polymeric jet. The morphology of the fibers deposited on the collector electrode was observed using SEM imaging. The conditions for formation of beaded fibers were studied. The sphere formation mechanism was observed for different parameters including polymer concentration, applied voltage, and needle to electrode distance.

Findings and Conclusions:

Observations of electrospinning of aqueous solutions of PEO at different concentrations yielded the following major conclusions:

1. As the concentration of the solution decreases, beaded fibers are formed. Further reduction in the concentration results in the generation of beads with spindle-like structures. This could possibly be attributed to the decrease in the viscosity of the polymer solution, and hence a decrease in the damping of the axis-symmetric disturbances along the jet surface.
2. Increasing the applied voltage and the traveling distance favors the formation of sphere-like structures with short tails.
3. Spheres of PEO were observed for the following test conditions: applied voltage = 30kV, gap = 0.23m and initial polymer concentration of 0.25% by weight.

ADVISER'S APPROVAL: Dr. K.A.Sallam